Democratic And Popular Algerian Republic

Ministry Of Higher Education And Scientific Research

Echahid Hamma Lakhdar University Of El-Oued

Faculty Of Technology

Department Of Process Engineering And Petrochemistry

Master's Thesis

In order to obtain a diploma of an Academic Master

In Process Engineering And Petrochemistry

Specialty: Chemical Engineering

Presented by:

Miss: Ounissi lnes

Miss: Ben nacib kenza

Miss: Zehouani Afaf

Miss: Khellout Ikram

Miss: Allal hayat

Theme

Bibliographic study: the influence of synthesis methods on the physico-chemical properties of perovskites

President	**Dr . BOUHRIRA Abdelaziz**	**M.C.B**	**El-Oued University**
Examiner	**Dr . HAMMAMI Hadia**	**M.C.A**	**El-Oued University**
Supervisor	**Dr. Fodil Hanane**	**M.C.A**	**El-Oued University**

University year: 2022/ 2023

Thanks

First and foremost, thanks and praise be to Allah Almighty

the Creator of mankind, the Bestower of intellect and eloquence who has

facilitated for us the means of success and has rescued us from the darkness of

ignorance into the light of knowledge He has guided us to accomplish this humble

work to Him belongs all praise until He is pleased, and to Him belongs all praise

even after His satisfaction.

We extend our heartfelt thanks and appreciation to Dr." Fodil Hannan"

our supervisor

for all the guidance, information, and advice she has provided us throughout our

work. We ask Allah to protect her, grant her good health and well-being.

We extend our sincere thanks and gratitude to our esteemed teachers

and everyone who has contributed to our education.

We also thank everyone who has helped us from near or far, even with a valid word or invitation.

إهداء

أهدي هذا العمل المتواضع إلى من كلله الله بالهيبة والوقار, وعلمني

العطاء بدون انتظار والذي أحمل اسمه بكل افتخار,أرجو من الله أن يمد في عمرك لترى ثمارا قد حان قطافها بعد طول انتظار , وستبقى كلماتك نجوم أهتدي بها اليوم في الغد وإلى الأبد إليك

أهدي هذا العمل والدي العزيز : عز الدين

كما أهديه إلى ملاكي في الحياة , وإلى معنى الحب والحنان والتفاني ,على بسمة الحياة وسر الوجود ,وإلى ما كان دعائها سر نجاحي وحنانها بلسم جراحي إليك أهدي عباراتي والدتي العزيزة : ليلى

إلى من حبهم يجري في عروقي , وشموعي أضاءت دربي إخواني :

منتصر بالله و محمد البشير

إلى من تذوقت معهن أجمل اللحظات وتقاسمت معهن حزني و سعادتي أخواتي : إيمان و أبنائها (محمد ياسين ' أحمد فراس),رحمة ,اسراء:

تحت اشراف الأستاذة الكريمة :فضيل حنان

الى كل أقاربي وكل من يعرفني كبيرا وصغيرا

(مع شكر خاص لخالتي الغالية هدى وعمتي العزيزة خيرة)

الطالبة: خلوط إكرام

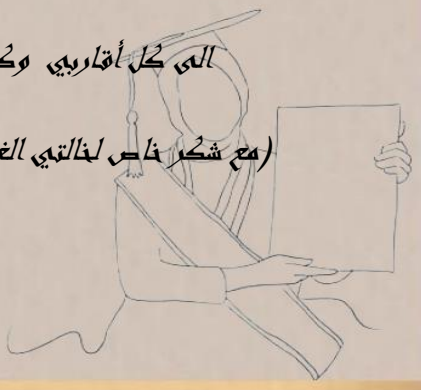

إهداء

أهدي هذا العمل إلى من أنار دربي وأعانني وتعب في تعليمي أغلى إنسان في هذا الوجود "أبي الغالي"

إلى من سهرت وتعبت في تعليمي، وأعانتني بدعواتها وصلواتها "أمي الغالية"

إلى رموز المحبة والوئام والتعاون إخوتي علي ,سعيدة,بيان

إلى كل أفراد عائلتي صغيرها وكبيرها و كل الأصدقاء والأحباب و الأقارب

إلى رفيقة الدرب والروح وزميلتي في هذا العمل

بن نصيب كنزة

و إلى كل من يعرفني، وساعدني ودعا لي.

ونسال الله ان يجعله نبراسا لكل طالب علم

الطالبة :ونيسي ايناس

إهداء

أهدي هذا التخرج إلى من علمني العطاء وإلى من أحمل اسمه بكل افتخار وأرجو من الله أن يمد في عمرك لترى ثمارا قد حان قطافها بعد طول انتظار "ابي الغالي"

إلى ملاكي في الحياة وإلى معنى الحب والحنان وسر الوجود وإلى من كان دعائها سر نجاحي أغلى الحبايب "امي الحبيبة"

إلى زوجي الذي شاركني لحظات التعب وشجعني إلى أن وصلت إلى هنا

إلى اغلى الحبايب اخواتي وسام ونسرين وصبرينة وسندي في الحياة اخوتي قدور وإبراهيم

إلى غاليتي ورفيقة الدرب وزميلتي في العمل الاغلى على قلبي ايناس ونيسي

إلى وردة قلبي وثمرة حبي ابنتي آيات

وإلى كل عائلتي واحبتي واصدقائي وكل من ساعدني للوصل الى هذا اليوم المميز

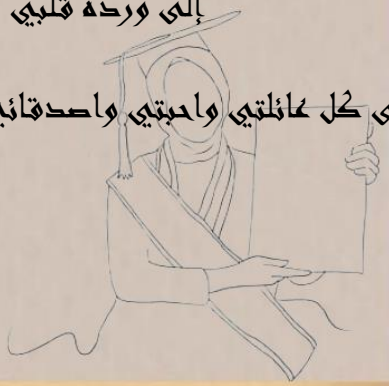

الطالبة :بن نصيب كنزة

إهداء

الحمد لله وحده والصلاة والسلام على رسول الله وعلى آله وصحبه ومن والاه أما بعد

بفخر وشرف أهدي ثمرة جهدي المتواضع إلى أغلى وأعز

انسانة في حياتي، الي من علمتني القوة والإسرار في تطور ذاتي إلى من جعل الله الجنة تحت قدميها ووقرها في كتابه

العزيز و كانت دعواها لي بالتوفيق تصادفني خطوة بخطوة في عملي، الى من ارتحت كلما تذكرت إبتسامتها في وجهي

نبع الحنان أعز ملاك على في الوجود جزاها الله عني خير الجزاء على حسن تربية حفظها الله لي وأدامها نورا لدربي.

"أمي العزيزة "أطال الله في عمرها

إلى من علمني ان الدنيا كفاح وسلاحها العلم والمعرفة ووهبني كل ما يملك حتى أحقق له أماله

"أبي الغالي "رحمه الله

الي الذين ظفرت بهم هدية من الأقدار وأرى السعادة في أعينهم وأنا بينهم وسندي في الحياة "اخوتي واخواتي" أتقدم بجزيل الشكر والاحترام لأساتذتنا الكرام في كلية التكنولوجيا قسم هندسة كيميائية ولأخص بالذكر لأستاذة مؤطر

"فضيل حنان "على كل ما قدمته وكانت خير عون لي في إنجاز هذه المذكرة

الي كل من لجأت اليه وكان سند لي وكل ما من سألته عن المعرفة زودني بها والي كل من في ذاكرتي وليس في مذكرتي.

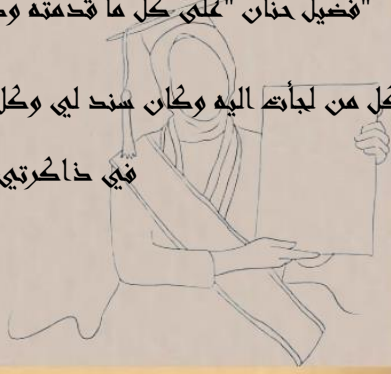

الطالبة : علال حياة

إهداء

إلى صاحب السيرة العطرة، والفكر المُستنير؛ فلقد كان له الفضل الأوَّل في بلوغي التعليم العالي (والدي الحبيب)، أطال الله في عُمره.

إلى من وضعتني على طريق الحياة، إلى من أُفضِّلها على نفسي،

التي دعمتني في كل قراراتي حتى وصلتو إلى هذه المرحلة

(أمي الغالية).

إلى قرة عيني و حبيبت قلبي (إبنتي إنتصار).

إلى إخوتي وأخواتي من كان لهم بالغ الأثر في كثير من العقبات والصعاب ممتنا لكم أعزائي.

إلى صدقاتي، ألاتي ساعدنني بكل ما يملكنا، لهن مني كل الحب وتقدير

وها أنا ذا أختم بحث تخرُّجي بكل مثابرة وصبر

أهديكم هذا البحث العلمي المتواضع

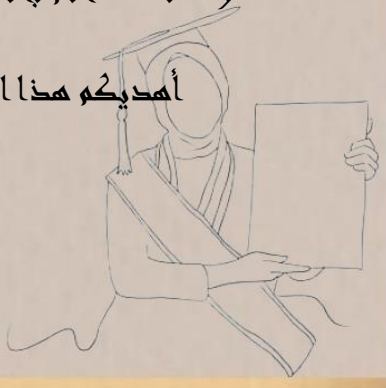

الطالبة: زهواني عفاف

Contents

Contents

List of tables

List of figures

List of figures

General introduction

General introduction

According to the numerous studies conducted between the 1950s and the present, manganites with a perovskite structure displayed a wide range of physical and structural characteristics [1]. Perovskite materials have attracted a lot of attention and have grown to be one of the most inspiring research topics[2].

Due to the fact that perovskites make up a significant portion of the earth's crust, it is highly desirable to study their physical characteristics. They exhibit a variety of intriguing physical characteristics that have applications in the fields of high thermoelectric power, ferroelectricity, superconductivity, charge order, spin-dependent transport, and massive magnetores, among other things. The most typical attribute of these materials is optics. These materials are excellent prospects for optoelectronics as well as being regularly employed as sensors and catalytic electrode substrates in fuel cells[3].

The nature of the A and B ions and their valence state are the primary determinants of the catalytic properties of perovskite type oxides, ABO3 [4-5].

Contrary to B-site ions, A-site ions are often catalytically passive, albeit their characteristics do affect the stability of the perovskite. However, structural modifications related to the formation of vacant oxygen sites and/or changes in the valence states of the original cations can result from the replacement of some of the ions at sites A or B by other heterovalents. [6-7].

There are various methods available for synthesizing oxides, particularly perovskite. The choice of preparation method plays a crucial role in determining the final structure of these materials. Among the methods commonly used are sol-gel, co-precipitation, and hydrothermal techniques. Solid-state technology is also employed, involving reactions in the solid state at high temperatures using oxide mixtures. To prepare perovskite using the solid-state method, the following steps are typically followed: selecting the raw materials, mixing them together, grinding the mixture, calcinating it, and re-grinding if necessary. In addition, wet synthesis methods, such as sol-gel and co-precipitation, offer distinct advantages. The sol-gel method allows for the development of a wide range of oxide compositions, making it highly versatile and attractive. On the other hand, the co-precipitation method, although an older technique, yields relatively homogeneous and non-crystalline compounds.

LaFeO3 is a prominent perovskite-type oxide because of its many uses in things like fuel cells, chemical sensors, magnetic materials, and membranes that can pass through oxygen.

After our study of the general introduction, this note consists of three chapters, namely:

General introduction

The first chapter presents a bibliographic review on mixed oxides: structure, physicochemical, electrical and electrochemical properties, as well as the applicatios of perovskite type oxides.

The second chapter deals with experimental techniques:preparation methods, physico-chemical characterization techiques.

The third chapter we conducted a comparative study of the LaFeO3 compound using Three different ways: sol-gel, hydrothermal, solid condition and we analyzed Using different technologies, including XRD, FTIR, ATD/ATG and SEM. Comparison of the vehicle's usesLaFeO3

References:

[1] Perca, Cristian. Structure cristalline et magnétique de perovskites RBaMn2O6-d (où d= 0 et 0.5). Diss. Université Paris Sud-Paris XI, 2005.

[2] CHOUIAH, Mr A. Etude Ab-initio des Propriétés structurales, optoélectroniques, thermodynamiques et magnétiques des pérovskites. Diss. Université de Mostaganem, 2019.

[3] Youcef, BENAISSA CHERIF. Structures Magnétiques des Pérovskites de type ABC3 Etude du premier principe. Diss. Université de Mostaganem, 2018.

[4-5] Fodil, Hanane. Etude physicochimique des oxydes mixtesBaFe1-x AlxO3. Diss. Université Mohamed Khider-Biskra, 2016.

[6-7] Fodil, Hanane. Etude physicochimique des oxydes mixtesBaFe1-x AlxO3. Diss. Université Mohamed Khider-Biskra, 2016.

[8] Abdellah, Mr BAHMANI. "Synthèse, caractérisation et propriétés électriques d'oxydes mixtes dans les systèmes Sr-Ca-Bi-O et Sr-Sn-Ti-O." en ligne]. Thèse de doctorat, université des sciences et de la technologie, Oran, 2012.[consulté le 24/05/2022]. Disponible à l'adresse http://www. univ-usto. dz/theses_en_ligne/doc_num. php? explnum_id 870 (2012).

[9] Abdellah, Mr BAHMANI. "Synthèse, caractérisation et propriétés électriques d'oxydes mixtes dans les systèmes Sr-Ca-Bi-O et Sr-Sn-Ti-O." en ligne]. Thèse de doctorat, université des sciences et de la technologie, Oran, 2012.[consulté le 24/05/2022]. Disponible à l'adresse http://www. univ-usto. dz/theses_en_ligne/doc_num. php? explnum_id 870 (2012).

[10] BENAICHA, Abdelhakim. Synthèse et propriétés des oxydes LaFe1-xCuxO3. Diss. Université Mohamed Khider-Biskra, 2018.

Chapter I: General presentation on perovskites

Chapter I: General Presentation on Perovskites

Generality on perovskites:

I -1-Introdution:

Mineral perovskite has the chemical formula CaTiO3. It was found in mineral formations in the Ural Mountains in 1839 by the Prussian mineralogist Gustav Rose. It was given the Count Lev Aleksevich von Petrovski mineralogist's name. The density of natural perovskite crystals is between 4000 and 4300 kg/m3, and their hardness ranges from 5.5 to 6. They usually have impurities that make them appear dark brown to black, but when they are pure, they are clear and have a refractive index of roughly 2.38. Its orthorhombic crystal structure was later discovered, despite the fact that it was first thought to have a cubic structure (Table 1.1).

Perovskite, like many other minerals, has given rise to a class of substances known as perovskites, which have a generic formula that is very similar to or descended from the formula ABX3. Hundreds of known chemicals at this time adopt the perovskite structure. Interestingly, Bridgmanite (Fe,Mg)SiO3, a mineral with a perovskite structure, makes up 38% of the content of the Earth's interior and is the most common solid phase there. Despite occurring at depths of roughly 660 to 2900 km, it can only be stable at extreme temperatures and pressures, hence it cannot be found on the Earth's surface.

To some extent, the variety of perovskite family phases can be rationalized by considering perovskites as simple ionic compounds, where A usually represents a large cation, B represents a medium-sized cation, and X represents an anion **[1].**

Table I.1 Representative ABX_3 perovskite phasesa

Phase	Space group[b]	Unit cell		
		a (nm)	*b* (nm)	*c* (nm)
1, 2				
$AgMgF_3$	C, $Pm\bar{3}m$ (221)	0.41162		
$CsPbI_3$	C, $Pm\bar{3}m$ (221)	0.62894		
$KCuF_3$	T, *I4/mcm* (140)	0.56086		0.76281
$KMgF_3$	C, $Pm\bar{3}m$ (221)	0.39897		
$KZnF_3$	C, $Pm\bar{3}m$	0.40560		
$NaMgF_3$	O, *Pbnm* (62)	0.48904	0.52022	0.71403
$NaFeF_3$	O, *Pnma* (62)	0.56612	0.78801	0.54836
NH_4ZnF_3	C, $Pm\bar{3}m$ (221)	0.41162		
1, 5				
$KTaO_3$	C, $Pm\bar{3}m$ (221)	0.40316		
$KNbO_3$	O, *Amm2* (38)	0.3971	0.5697	0.5723
2, 4				
$SrTiO_3$	C, $Pm\bar{3}m$ (221)	0.3905		
$BaTiO_3$	T, *P4mm* (99)	0.39906		0.40278
$CaTiO_3$	O, *Pbmn* (62)	0.54035	0.54878	0.76626
$BaSnO_3$	C, $Pm\bar{3}m$ (221)	0.4117		
$CdSnO_3$	O, *Pnma* (62)	0.52856	0.74501	0.51927
$CaIrO_3$	O, *Pbnm* (62)	0.52505	0.55929	0.76769
$PbTiO_3$	T, *P4mm* (99)	0.3902		0.4143
$PbZrO_3$	O, *Pbam* (55)	0.58822	1.17813	0.82293
$SrCoO_3$	C, $Pm\bar{3}m$ (221)	0.3855		
$SrMoO_3$	C, $Pm\bar{3}m$ (221)	0.39761		
$SrRuO_3$	O, *Pnma* (62)	0.55328	0.78471	0.55693
$(Fe,Mg)SiO_3$	O, *Pnma* (62)	0.5020	0.6900	0.4810
3, 3				
$BiFeO_3$	Tr, *R3c* (161)	0.55798		1.3867
$BiInO_3$	O, *Pnma* (62)	0.59546	0.83864	0.50619
$ErCoO_3$	O, *Pbnm* (62)	0.51212	0.54191	0.73519
$GdFeO_3$	O, *Pbnm* (62)	0.53490	0.56089	0.76687
$HoCrO_3$	O, *Pnma* (62)	0.5518	0.7539	0.5245
$LaAlO_3$	Tr, *R3c* (161)	0.53644		1.31195
$LaCoO_3$	Tr, $R\bar{3}c$ (167)	0.54437		1.30957
$LaMnO_3$	O, *Pbnm* (62)	0.55367	0.57473	0.76929
$LaTiO_3$	O, *Pbnm* (62)	0.5576	0.5542	0.7587
$NdAlO_3$	Tr, $R\bar{3}c$ (167)	0.53796		1.31386
$PrRuO_3$	O, *Pnma* (62)	0.58344	0.77477	0.53794
$YbMnO_3$	O, *Pbnm* (62)	0.52208	0.58033	0.73053
4, 5				
$ThTaN_3$	C, $Pm\bar{3}m$	0.4020		

I.2. Ideal Perovskite structure

Perovskite oxide, which is typically denoted by the chemical formula ABO3, refers to a large variety of mixed oxides. This structure's crystal lattice is made up entirely of ABO3 molecules, where A stands for a large cation with a coordination number of 12 (such as Ba, Ca, Pb, Rb, Sr, Na, K...) and B for a smaller, higher-charged cation with a coordination number of 6 (such as Ti, Sn, W, Zr, Nb, Ta, etc.). O is used to represent the oxygen ion. An ideal cubic lattice group with the space group Pm3m, where the A atoms are, describes the structure of a perovskite.

occupy the corners of the cube, the B atoms occupy the center, and the oxygen atoms O are located at the faces of the cube **[2].**

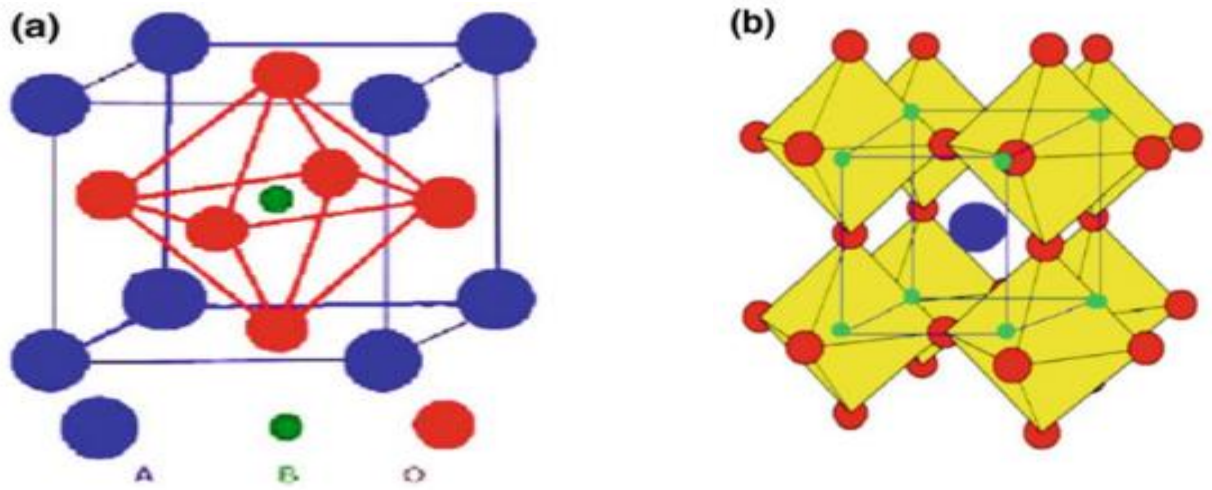

Figure. I.1: a) Unit cell of a cubic ABO_3 perovskite structure and

b) framework of an ABO_3 perovskite[3].

Oxygen octahedra that are corner-shared and span three dimensions make up the structure. We can distinguish between two different types of structures based on the atoms that occupy sites A and B:

1. ABO3 formations in which the same type of atom occupies both positions A and B. Simple perovskites include these structures, which include PbTiO3, BaMnO3, and KnbO3.

2. Structures with two different atom types occupying one of locations A or B. These are referred to as complex perovskites, with La0.8Sr0.2CoO3, PbMg0.33Nb0.67O3, and PbCo0.25Mn0.75O3 serving as illustrative examples [2].

The ideal perovskite phases with Pm3m symmetry are non-polar. However, in lower symmetry systems, the lattice undergoes slight and varied deformations, ranging from quadratic to orthorhombic or rhombohedral types. These deformations occur due to a slight displacement of the oxygen octahedra with an off-centering of

the B ion in specific directions determined by the symmetry elements of the new crystalline system **(Figure I.2).** These directions are as follows:

- the 3 order axes 4 (A_4) in the quadratic phase;
- the 6 order axes 2 (A_2) in the orthorhombic phase;
- the 4 order axes 3 (A_3) in the rhombohedral phase.

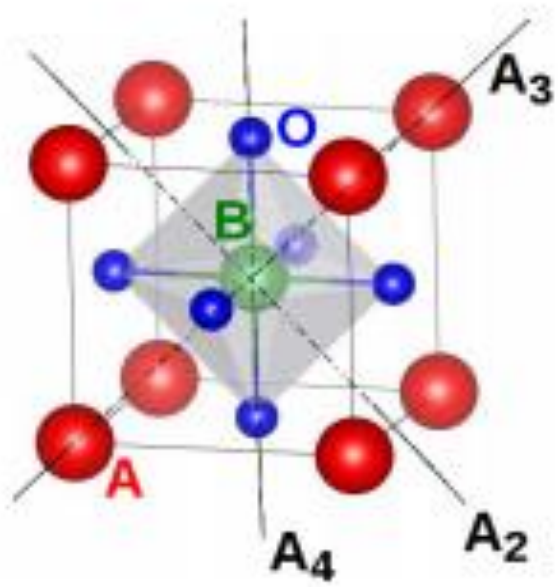

Figure I. 2: Directions of deformation due to the displacement of the B ion in the octahedron **[4].**

The displacements of the B-ion in the perovskite structure are a result of significant changes in the binding forces, specifically an increase in the covalent character of the B-O bonds. These changes in the bond character lead to the rearrangement of the oxygen octahedra.

The settlement of the oxygen octahedron framework occurs when the size of the ion occupying site A does not allow for the filling of all the available space in the cubo-octahedral site. In such cases, the A-O distance is minimized by rotating the octahedron around its center of gravity and displacing it relative to the A ion **[2].** This displacement helps optimize the A-O distance and achieve a more stable configuration within the perovskite structure.

I-3-Distortions of the ideal structure

As discussed earlier, the cubic symmetry and Pm3m space group of the ideal perovskite phases result in non-polar properties. The ideal structure can, however, be deformed or distorted to produce polar phases, which have lesser symmetries. Depending on elements like the size and makeup of cations A and B as well as the tolerance factor, these distortions and phase transitions may take place in the elementary lattice of the ideal cubic structure. The particulars of the octahedral rotations govern the structural arrangements that result from these distortions, which include orthogonal, rhombohedral, tetragonal, monoclinic, and triclinic [5] **(Table I.2).**

Table I.2: The different symmetries adopted by the Perovskite structure according to the tolerance factor t **[6].**

T	Symétrie observée
$\tau > 0.85$	**Fluorine ou hexagonale**
$0.85 < \tau < 0.9$	**Orthorhombique**
$0.9 < \tau < 1$	**Rhomboédrique**
$\tau = 1$	**Cubique**
$1 < \tau < 1.06$	**Hexagonale**

Three mechanisms responsible for these deformations have been identified by Megaw is:

*Octahedron deformation (BO_6).

*Displacements of the B ion in the octahedra of oxygen or the A ion in the

cubic octadres of oxygen.

* Rotation of oxygen octahedrons relative to each other (inclination of octahedrons) **[5].**

I-4-condition of stability of a perovskite structure

The difference in electronegativity between cations and anions, as well as the ionic radii, are both necessary for perovskite stability. The degree of ionic interaction between anions and cations and the tolerance factor are two important factors that impact perovskite's stability [7].

- **Ionicity of links:**

The stability of an ABO3 perovskite structure can be determined by comparing the electronegativity of the various ions. In a composition like ABO3, the degree of ionic bonding is determined by computing the electronegativity differences using the Pauling scale. This measures the compound's ionic nature.

$$\bar{x} = \frac{XA-O+XB-O}{2}$$

where $X_{A\text{-}o}$ O and $X_{B\text{-}O}$ are the electronegativity differences between A and B cations and associated oxygens. The perovskite structure is more thermally stable than the links involved have a strong ionic character.

- **tolerance factor**

The relationship was initially used by Goldschmidt in 1926, who suggested using it to forecast the likelihood that two ions will combine to form a perovskite structure phase. Since there weren't many crystal structures known at the time of this suggestion, ionic radii were employed in place of explicitly measured bond lengths. According to Goldschmidt's rule, it is believed that the cations must simply touch the surrounding anions in order for a stable structure to form. This presumption served as the foundation for an understanding of perovskite stability that was based on the ions' respective sizes.

$$t = \frac{(rA+ro)}{\sqrt{2}(rB+ro)}$$

where **t** is called the tolerance factor, rA is the radius of the cage site cation, rB is the radius of the octahedrally coordinated cation and rX is the radius of the anion.

Goldschmidt's proposal was that a perovskite structure phase would form if the value of the tolerance factor, **t**, was close to 1.0 **[1].**

expressions presented in the figure. In the ideal case the relationship between these two expressions must equal 1.

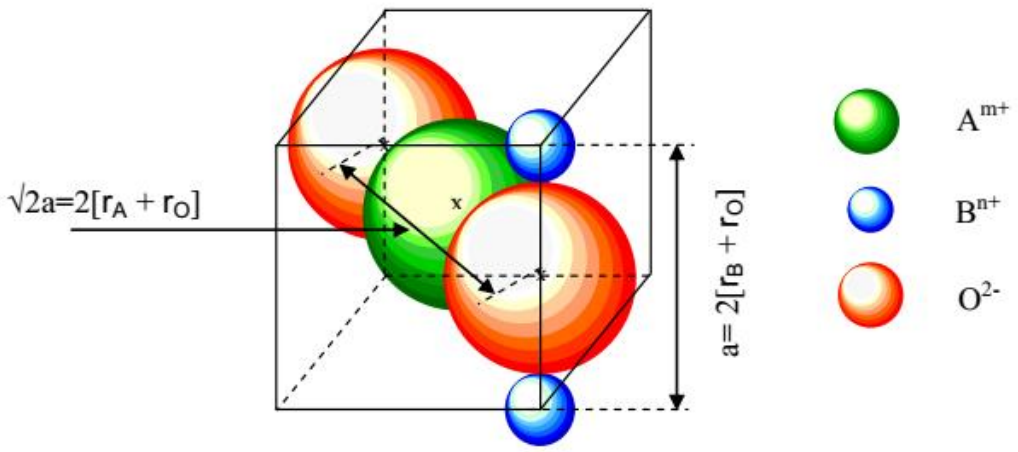

Figure. 1.3: In cubic perovskite ABO_3, the axes of the mesh are described by both **[6].**

I-4-1Tetragonal Perovskit

$BaTiO_3$ is a well-known example of a tetragonal perovskite, which exhibits ferroelectric properties at room temperature. Its unit cell parameters are a = 3.994 Å, c = 4.038 Å, and Z = 1. Within the structure, the TiO_6 octahedra undergo slight distortion. One Ti-O link is at 1.86 Å, four are at 2.00 Å, and the longest bond is at 2.17 Å.

In $BaTiO_3$, the barium ion is coordinated by four oxygen atoms at 2.80 Å, four at 2.83 Å, and four others at 2.88 Å. In the iso-type structure of $PbTiO_3$, the TiO_6 polyhedra exhibit greater distortion compared to $BaTiO_3$. This phenomenon can be attributed to the higher polarization power and the larger ionic **[8].**

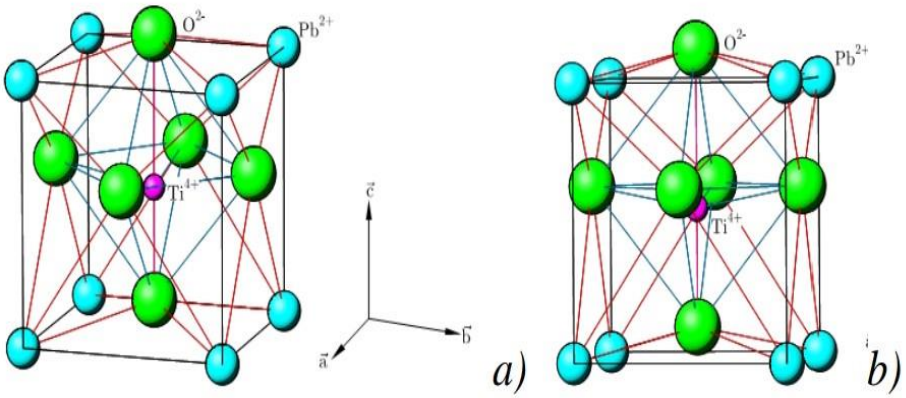

Figure 1.4 Tetragonal Perovskit **[9].**

I-4-2Perovskite Rhombohedral

The cubic lattice may somewhat bend toward the rhombohedral lattice in some materials. If the unit cell does not expand as a result of this deformation, it can be indexed to a different cell that has one or two unit formulas, with rhombohedral angles of 90° and 60°, respectively. The bigger unit cell with a 60° angle is usually accommodated by the anions moving their places accordingly.

Rhombohedral perovskite structures can be found in materials like LaAlO3, PrA1O3, LaNiO3, and LaCoO3. At room temperature, LaCoO3 has a rhombohedral shape. It does, however, go through two phase changes at high temperatures, changing from R3c to R3, into another rhombohedral phase. In addition, spin-up and spin-down Co(III) ions are organized in alternating planes (111) with trivalent cobalt ions. The space group R3 is retained in the second transition, which takes place above 937°C, although the angle suddenly shifts from 60.4° to 60.0° [10].

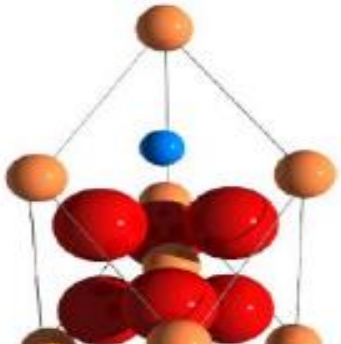

Figure 1.5: Perovskite Rhombohedral [11].

I-4-3Perovskite Orthorhombic:

One of the most illustrious instances of distorted orthorhombic perovskites is the GdFeO3 structure. Its lattice parameters are as follows: a = 5.346, b = 5.616, and c = 7.666 with a total of 4 formula units per unit cell (Z = 4). Its space group is Pbnm. The cubic pseudocubic lattice is related to these parameters in the following way: a = b 2a0, and c 2a0.

The FeO6 octahedra are bent and deformed in the GdFeO3 structure. Additionally, the GdO12 polyhedra show notable coordination and distortion (8 + 4). NaUO3, NaMgF3, LaYbO3, and various lanthanide compounds, such as LnCrO3, LnGaO3, LnFeO3, LnMnO3, LnRhO3, and others, also adopt this orthorhombic-distorted structure [10].

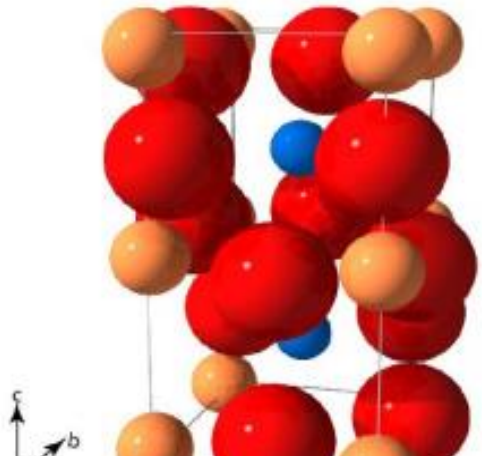

Figure 1.6: Perovskite Orthorhombic **[11]**

I-4-4Monoclinic and Triclinic Perovskite:

Perovskite structures have been described in a variety of forms, including monoclinic structures (like AgCuF3 and CsPbI3, PbSnO3, BiCrO3, etc.) and single mesh structures (like BiMnO3 and BiScO3). In some instances, triclinic formations have also been seen. These cell characteristics, however, were frequently discovered to be pseudocells of a true multiple cell. As an illustration, the phases of GdFeO3 were frequently categorized using a pseudomonoclinic mesh where a, b, a, and 90° were present [2]. This suggests that the measured cell characteristics are approximations or distortions of the crystal lattice, which differ from the genuine symmetry of the structure.

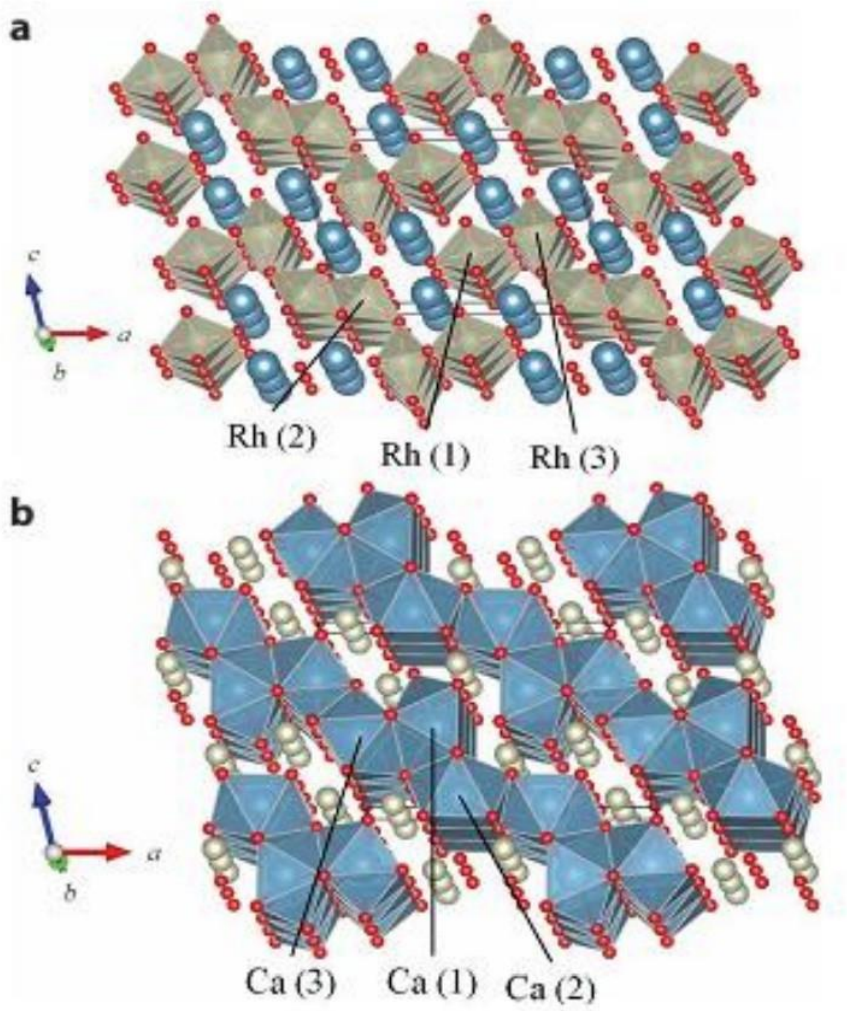

Figure.1.7. Monoclinic and Triclinic Perovskite**[9].**

$SrLaCuNbO_6$ and $SrLaCuTaO_6$ are Jahn_Teller distorted double perovskites with complete B_site ordeing. The crystal structure of $SrLaCuTaO_6$ has been solved by refinement of neutron powder diffraction data at (triclinic),573(monoclinic) and 923 k (body-centered monclinic).

I-4-5 Polymorphism:

Numerous polymorphism variations that many perovskite-type materials display, as was previously indicated, have a considerable impact on their physical characteristics and uses. BaTiO3 and KNbO3 are two prominent examples, both of which change as the temperature rises:

Rhombohedral ↔ orthorhombic ↔ tetragonal ↔ cubic

These phase changes are reversible and all these polymorphic forms have a pseudo cubic single mesh with a ~ 4 Å. It should be noted that the three forms are lower temperature ferroelectric **[2].**

I-5-Stoichiometric appearance of the perovskite structure :

Based on the cationic valences in simple ABO_3 oxide systems, the following classification can be made:

[1+ 5]=$A^{I}B^{V}O_3$

[2 + 4] = $A^{II}B^{IV}O_3$

[3 + 3] = $A^{III}B^{III}O_3$

Only these three types cover a wide range of compounds . However, a great many other possibilities arise when we consider cation structures Mixed type:

$A_{1-x}A_xBO_3$, $AB_{1-x}B'_xO_3$, $A_{1-x}A_x$ $B_{1-y}B'_yO_3$, $A_2B'O_9$, etc. On the other hand, many possible stoichiometry other than ABO_3 can be imagined, once defects are presented **[12].**

I-6 Defects in the perovskite structure

Despite the idealized notion of a flawless crystal, which consists of an unbroken and unlimited arrangement of atoms, ions, or molecules, imperfections are inherent in real crystals. In truth, each and every crystal has flaws [13]. In essence, a defect can be thought of as any departure from the crystal's lattice or structure [14].

I-6-1 Description of defects in crystals

In theory, any deviation from a crystal's painstakingly planned structure might be categorized as a flaw. Intrinsic flaws are those that develop within a purportedly pure solid and significantly affect its properties. On the other hand, an extrinsic flaw is when a foreign substance is incorporated into the major constituent's matrix. Point defects are defined as small regions of disorder that are randomly distributed throughout the crystal, as opposed to ordered defects that result in broad defects like crystallographic shear planes [15].

I.6.2. Spot defects:

Individual atoms are the main focus of punctual flaws. Although an atom does have a certain amount of space to occupy, this space is insignificant in comparison to the crystal's total volume. As a result, it can be roughly described as a point with no dimensions [16].

- **Gap:** a gap (vacancy); it is the absence of an atom. For example, a gap Cationic therefore has a negative charge in the crystal.
- **Interstitial:** The presence of a network atom between atoms. The presence of a foreign atom between the atoms in the network is called an interstitial solid solution.
- **Substitution:** The presence of a foreign atom instead of an atom in the network a solid substitution solution.

- **Electrical charge failure:** One crystal site has a negative charge (free electron) or more positive (electron hole) than other sites of the same type.

- **Antisite defects:** If the crystal is an ordered crystal, that is to say formed of several types of atoms with strict chemical alternation، so there may be defects antisite, that is, atoms that are well at a node in the network but which break the chemical regularity.

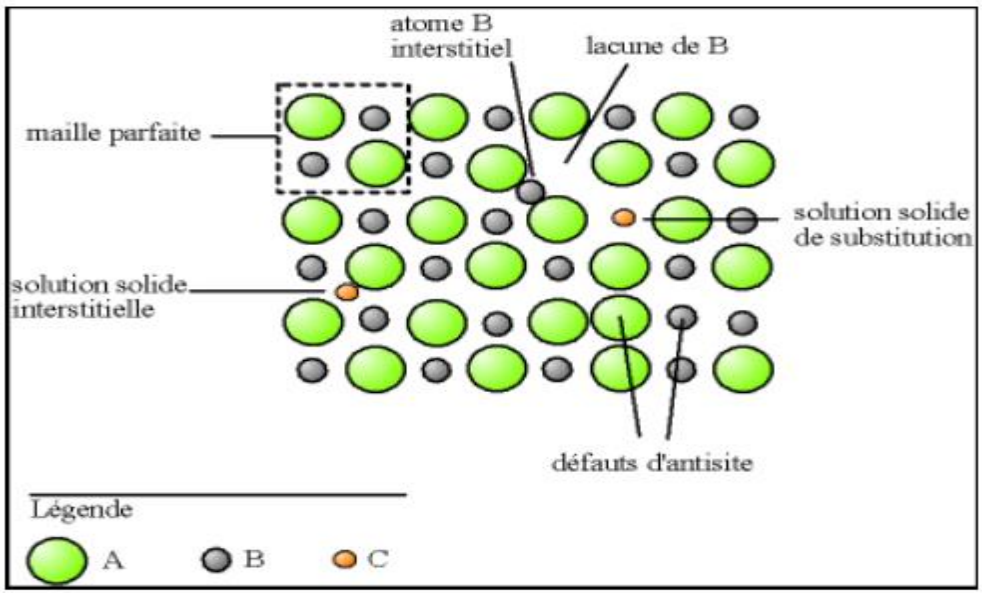

Figure 1.8. Example of spot defects in an ordered crystal AB. **[17]**

I.6.3. Association of point defects

Schottky defect :

illustrates a relationship between a cation gap and an anionic shortfall in ionic crystals[18].

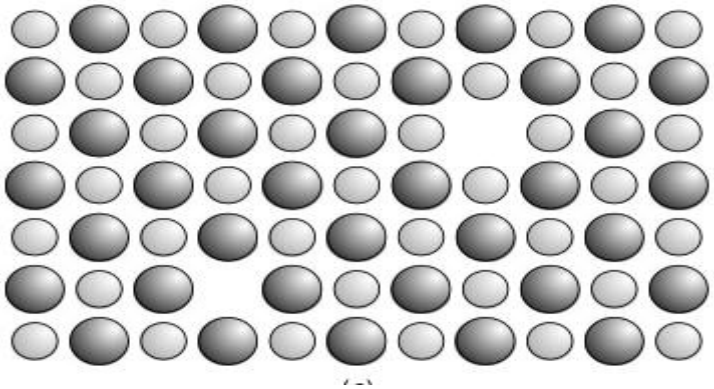

Figure 1.9 image of a Schottky Defects **[19]**

- **Defect of Frenkel :**

An interstitial defect occurs when an atom moves from its normal position within a crystal and settles in an interstitial site. Only cations can move into interstitial places in the case of an ionic crystal since they are smaller than anions [18].

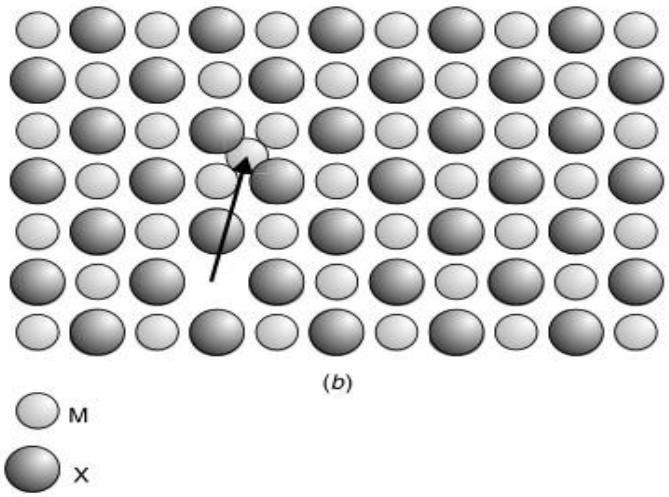

Figure 1.10 image of a Frenkel Defects **[19]**

- **Pile of defects :**

More complicated groups of defects, frequently referred to as "clumps" or "complexes," can also exist inside a crystal structure in addition to individual flaws [18].

I.6.4 . Representations of point defects:

To represent the point defects in the crystals, we use the notation of Kroger andVink:

The rating describes:

The chemical nature of the species (gap, atom, ion), The position of the species (inserted in a crystallographic site, interstitial), The relative load of the defect.

A punctual defect is thus noted xcy with:

X the chemical nature, “V” for a gap, “e” for a free electron.

Y the position, either the name of the atom or ion it replaces, or “i” for interstitial.

c the relative charge, an apostrophe “’” for a negative relative charge, a point “.” for

a positive relative charge, nothing or an “x” cross for a neutral charge **[20].**

I.6.5. Mechanism of defect diffusion:

Due to the influence of thermal energy, atoms in a solid can undergo jumps from one lattice site to a nearby site, resulting in their gradual migration. Displacements within the crystal lattice, whether through vacancies or interstitials, tend to be slower compared to movements that occur on the surface or at grain boundaries (refer to the figure). This phenomenon is referred to as self-diffusion when atoms of a pure or majority element displace, while heterodiffusion is used to describe the movement of solute atoms within a solvent. In all materials, the atomic mobility caused by thermal energy and its associated agitation is a prevalent phenomenon **[21].**

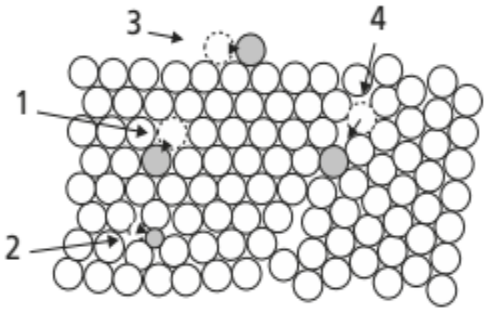

Figure I .11 : Dissemination mechanisms most common in a crystalline solid.

1. Lacunal mechanism
2. interstitial mechanism (possible only for small solutes);
3. diffusion surface
4. diffusion in a grain seal.

a. Lacunal mechanism:

In this mechanism, there can be dissemination only when a deficiency occurs in proximity of a surrogate impurity, the sites can then be exchanged **[22].**

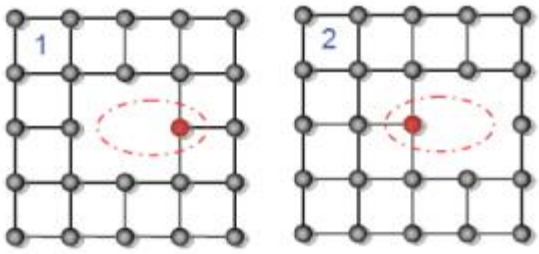

Figure 1.12 : diffusion Lacunal

b. interstitial mechanism:

The figure illustrates the following mechanism: In (1), there are two silicon atoms occupying a single lattice site, forming a "dissociated auto-interstitial." If this dissociated auto-interstitial approaches a surrogate impurity in (2), an interaction can occur, resulting in the formation of an interstitial impurity known as a "dissociated mixed interstitial." This dissociated mixed interstitial can propagate over long distances, resembling the diffusion of an impurity/autointerstitial pair. Following a jump (or multiple jumps) in (3), the mixed interstitial dissociates in (4) to reform a "dissociated auto-interstitial."

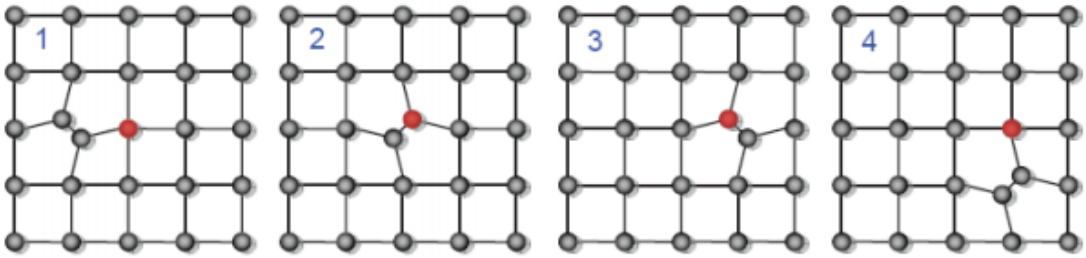

Figure 1.13 : diffusion interstitial

II. Properties of Perovskite Materials

II.1.Introduction

In recent years, there has been a growing interest in Perovskite-type materials due to their significant potential in various applications such as solid fuel cells, solid electrolytes, fixed resistors, actuators, electromechanical devices, transducers, and more. These materials possess unique crystalline structures, magnetic properties, electrical conductivity, piezoelectric and electro-optical characteristics, catalytic activity, and gas sensitivity, among others **[23].**

II.2.Electrical properties

The remarkable properties of perovskite-type materials include high temperature superconductivity, the capacity to convert mechanical pressure or heat into electricity (piezoelectricity), the capacity to catalyze chemical reactions, and the ability to undergo abrupt changes in electrical resistance when exposed to a magnetic field. The electrochemical behavior of these oxides as electrode materials in aquatic conditions has been the subject of numerous studies.

These experiments have demonstrated the important electrocatalytic function of perovskite-based electrodes, particularly at ambient temperature, in oxygen-related processes [24].

II.3. Catalytiques proprietes

The spectroscopic domains of magnetism, optics, vibrations, electricity, and catalysis are among the many spectroscopic domains in which ABX3 perovskites display a variety of intriguing features. With an emphasis on the influence of the structure and surface composition on catalytic capabilities, the use of perovskite oxides in oxidation catalysis will be highlighted in this context [25].

II.4.Fuel cells

II.4.1. History

The earliest explorations into fuel cells were made by William R. Grove in 1839. Christian Friedrich Schoenbein made important contributions before that by presenting proof of water electrolysis, which is regarded as the opposite process of fuel generation in a battery. However, additional development didn't occur for nearly a century. The first fuel cell prototypes with a few kilowatts of power were developed in the 1950s, in large part because to Francis T. Bacon. This delay can be ascribed to the development of alternative energy generation techniques as well as the high cost of the components used in batteries and fuel cells [26].

II.4.2. Operation of a solid oxide fuel cell (SOFC):

The basic structure of an SOFC consists of a solid electrolyte (usually a ceramic) positioned between an anode and a cathode. Fuel is delivered to the anode and oxidant, typically air, is delivered to the cathode. The electrodes are solid porous structures that allow the fuel and air to diffuse to the electrolyte and the products of the electrochemical reaction on the anode side to diffuse away from the electrolyte. The electrolyte conducts the oxygen ions formed by the electrochemical reduction of molecular oxygen from the cathode side to the anode side of the SOFC. Fuel diffuses through the anode to the anode/electrolyte interface. Here it reacts catalytically with the oxygen ions, releasing electrons that are transported through an external circuit, producing electricity. Individual cells are linked with a metallic interconnect in electrical series to increase voltage and power and can be stacked to achieve an optimal stack size. A number of stacks can be arrayed within an enclosure to form an SOFC module **[27].**

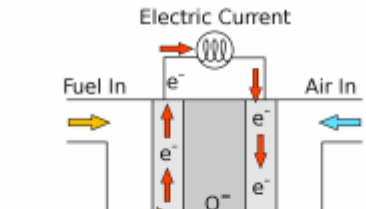

Figure II.1: Solid Oxide Fuel Cell (SOFC) model diagram use to represent system (Solid oxide fuel cell, 2022) **[28].**

The electrochemical interaction between oxygen and hydrogen, which occurs in each fuel cell individually, through the catalyst electrode couple, enables the battery to generate current and electricity. In order to make water, hydrogen is first oxidized. This is discernible from the subsequent redox reaction.

$$H_2 + 1/2\ O_2 \rightarrow H_2O$$

The oxygen is then absorbed onto the other electrode into the cell. This is the direction at which the electrons are flowing. This ionization reaction can be seen below.

$$1/2\ O_2 + 2e^- \rightarrow O^{2-}$$

Finally, the negatively charged oxygen flows through the electrolyte back to the hydrogen electrode. The hydrogen and oxygen combine to create water.

$$2H^+ + O^{2-} \rightarrow H_2O$$

By placing a solid electrolyte ceramic material between an anode and a cathode. fuel is delivered to the anode and oxidant while air is delivered to the cathode. The electrodes are porous materials that allow both fuel and air to diffuse through. When molecular oxygen is reduced from the cathode side to anode side, fuel diffuses through the anode and interacts with the oxygen ions, releasing electrons and producing electricity (Solid Oxide Fuel Cells, n.d.).

II.5. conductive

Perovskites having the formula ABO3, in which A is commonly a rare earth element and B is a transition metal, are used as the stack cathodes in SOFCs. These substances are principally electronic conductors or primarily electronic materials. Because they must be carefully assembled and operated in extremely physico-chemical and thermal conditions, SOFCs are extremely complex technological devices. Combining porous electrodes, compact electrolytes, and connecting materials results in complexity. There are three different types of conductors in SOFCs for current transport [29]:

- By electrons
- By charged atoms.
- By charged electrons and atoms.

II.5.1. Oxygen reduction:

Fuel cell cathode (SOFC); is the seat of oxygen reduction; according to the following reaction:

$$\text{½ O2} + 2e^- \rightarrow O^{-2} \qquad \textbf{(1)}$$

So it is porous to allow the gaseous oxygen to diffuse to the point of reaction. The gas is adsorbed and then dissociated and reduced to O^{2-} ions due to the presence of oxygen gaps. The where this reaction occurs and where the electrons of the cathode are simultaneously present, Electrolyte oxygen gaps and gaseous oxygen are called triple or triple point contact(TPB for Triple Phase Boundary). This process is mapped on the figure and may be summarized by reaction (2) according to the notation of Kroger and Vink **[30].**

$$1/\ 2O_2 + 2é + V_O^{\cdot\cdot} \rightarrow O^x_0 \qquad \textbf{(2)}$$

Where $Vo^{\bullet\bullet}$ represents an oxygen deficiency of the electrolyte and O_O^X an oxygen atom inserted into theelectrolyte network in normal position.

Figure II.2: Triple point (TPB)

II-5-2- electrode matarials with Mixde conductors:

The simultaneous presence of oxygen from the gas phase, electrons in the cathode and oxygen gaps in the electrolyte limit the surface of the reaction zone.

A possible improvement is to use a conductive cathode Mixed Ionic Electronic (Mixed Ionic Electronic Conducting, MIEC), allowing to delocalize the reduction of oxygen on the whole surface the cathode and thus reduce the electrode surges **(figure II.3).[31]**

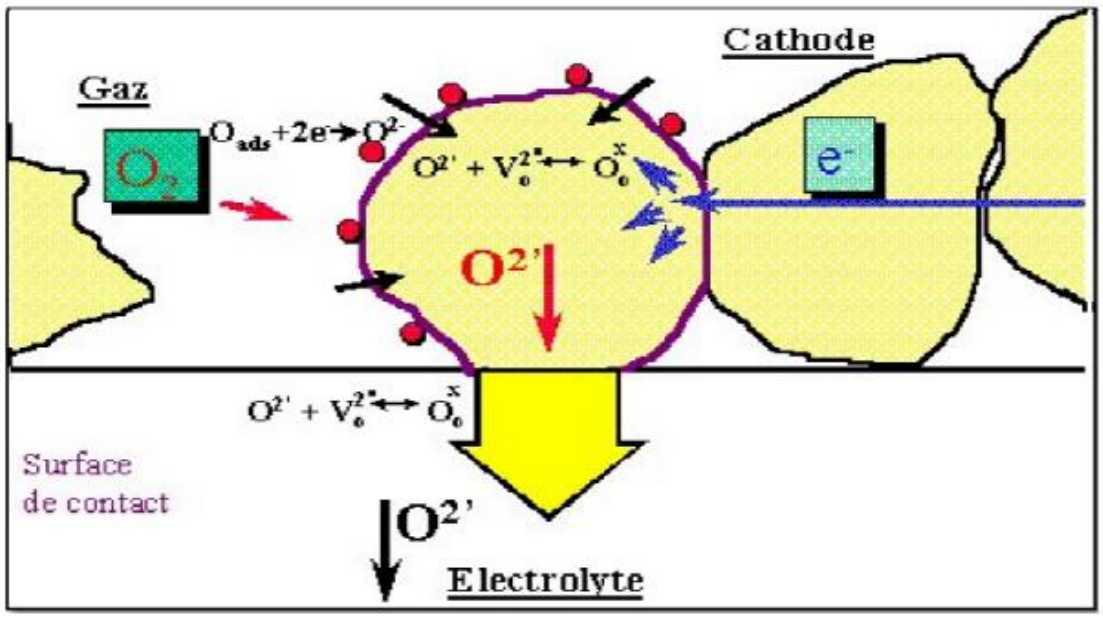

Figure II.3: diagram of composite conductive electrode materials

In addition to facilitating the transport of electrons, the cathode material in a solid oxide fuel cell (SOFC) must also exhibit good ionic conductivity. This allows O^{2-} ions to migrate from the cathode to the electrolyte. Furthermore, the cathode material should possess excellent electrocatalytic properties for oxygen reduction. The efficiency of oxygen exchange at the surface of the cathode material is quantified by the oxygen exchange coefficient (k).

Most studies on mixed conductors in SOFCs focus on oxides of the Perovskite type with the formula ABO_3. The cations occupying the A-site typically belong to the family of rare earth elements such as lanthanum, gadolinium, praseodymium, neodymium, samarium, or cerium.

The B-site cations are transition metals, including chromium, manganese, cobalt, and others. One commonly studied material is $LaCrO_{3-\delta}$.

Recently, new perovskite-structured materials have been developed, expanding the range of potential cathode materials for SOFCs. These advancements contribute to ongoing research and development efforts aimed at enhancing the performance and efficiency of SOFC technology.

II-5-3-Influence of over-stoichiometry in oxygen:

Ion conductivity can be improved by the existence of a oxygen stoichiometry.

The overall electrochemical reaction which occurs at the cathode of a SOFC battery is the reduction of oxygen:

$$1/2\ O_2 + 2e^- \rightarrow O^{2-}$$

It can be broken down into several stages, the main ones being schematically represented in the figure. It should be noted immediately that the existence of all of these steps are not fully demonstrated to date **[32].**

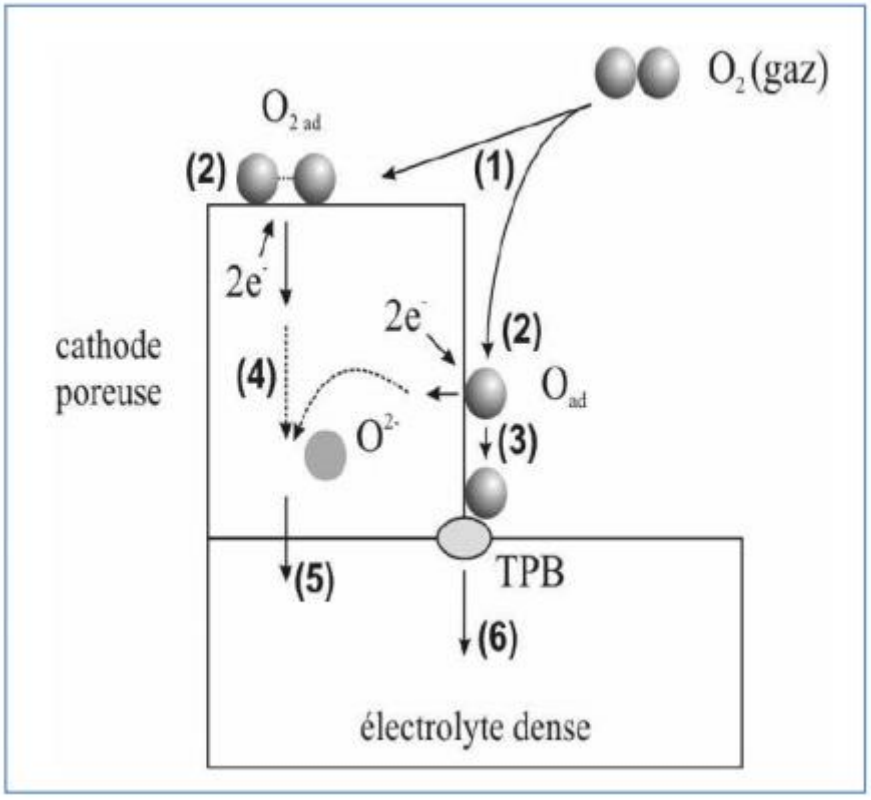

Figure II.4: Schematic representation of electrochemical oxygen reduction The cathode/electrolyte interface

1. diffusion of O_2 gas molecules
2. Adsorption, dissociation, réduction d'O_2 and insertion of ions O^{2-} in the cathode
3. surface diffusion of adsorbed oxygen

4. core diffusion of O^{2-} ions
5. transfer of O^{2-} ions from the cathode to the electrolyte
6. incorporation into the electrolyte of oxygen adsorbed via the triple TPB point

II.6.Electrochemical properties

Oil prices, which are the main source of energy, are rising along with the global energy consumption. One of the solutions to this issue is the development of new technologies with high power generation capabilities and other sources of renewable energy. Due to its advantages for the environment, electrical power, and high energy, fuel cells are the most promising of these new clean and efficient technologies. Additional research is being done right now on nanomaterials in the realm of catalysis with the goal of creating novel, less-expensive, non-poisonous catalysts that also increase responsiveness and selectivity. Therefore, research has concentrated on lowering the operating temperature at values between 600°C and 800°C [33].

II.6.1. Introduction to Electrochemical Techniques

Electrical quantities, current and potential, which are averaged over the entire surface, are used in the majority of electrochemical procedures. If there are surface, for example, places that are significantly more active than others, the data acquired under these settings are challenging to interpret. Heterogeneities include things like intergranular corrosion, localized corrosion, and the simple presence of spot flaws on a coating.

To further explore these occurrences In reality, numerous approaches have been created recently, including the vibrating electrode, microcell, Kelvin probe, and electrochemical microscope. These methods are based on the application of microelectrodes, which can measure minute quantities (in current or potential) at specified points on the metal surface. [34]

REFERANCES

[1] Tilley, Richard JD. *Perovskites: structure-property relationships*. John Wiley & Sons, 2016.

[2] Mya, Omar Ben. *Synthèse et Caractérisation de la pérovskite La1-xSrxFe0. 7Ni0. 3O3*. Diss. 2015.

[3] Arul, Narayanasamy Sabari, and Vellalapalayam Devaraj Nithya. *Revolution of Perovskite*. Springer Singapore, 2020.

[4] Amisi, Safari. "Etude ab-initio d'oxydes antiferroélectriques de structure pérovskite." (2013).

[5] Aissat, Fares. *Synthèse, caractérisation et activité catalytique des matériaux de structure pérovskite*. Diss. 2019.

[6] Mahboub, Mohamed Sadek, and Ali Boudjada. "Synthèse, caractérisation par diffraction X et spectroscopie Raman des composés Ca1-xSrxFeO2. 5-δ (δ= 0, 0.5)." (2017)

[7] DJAHMOUM, Mourad. *Elaboration et caractérisation de matériaux appartenant au système Bi/La MnO3*. Diss. Universite Mouloud MAMMERI Tizi-Ouzou, 2020.

[8] Adaika, Kaltoum. SYNTHESE ET CARACTERISATION HYSICOCHIMIQUE DES OXYDES La Cr1-xCuxO3. Diss. Université Mohamed Khider-Biskra, 2015.

[9] Djani, Faiçal. *Etude physicochimique du système LaMM'O3 à base de métaux divalents et trivalents*. Diss. Université Mohamed Khider-Biskra, 2016.

[10] Youcef, BENAISSA CHERIF. *Structures Magnétiques des Pérovskites de type ABC3 Etude du premier principe*. Diss. Université de Mostaganem, 2018.

[11] Pan, Likun, and Guang Zhu, eds. Perovskite materials: synthesis, characterisation, properties, and applications. BoD–Books on Demand, 2016.

[12] Muller, Olaf, and Rustum Roy. "Crystal chemistry of non-metallic materials." *The Major Ternary Structural Families*. Vol. 4. Springer-Verlag New York, 1974. 143.

[13] Guiraldenq, Pierre. "Diffusion dans les métaux." *Techniques de l'ingénieur*.

[14] Bedjaoui Habiba, Djemai Nadjma. "Synthèse et caractérisation physico-chimique d'oxyde mixte de type pérovskite."

[15] J. F. Marucco, " chimie des solides ", EDP Siences ed., 2004.

[16] Smart, Lesley, and Elaine A. Moore. Introduction à la chimie du solide. Masson, 1997

[17] Farida Bouremmad« Les Manganites De Type Perovskite : Synthèse, Structure Cristalline Et Propriétés Electriques Et Catalytiques» Thése Doctorat Universite Mentouri – Constantine 17 / 03 / 2010.

[18] Raccah, P. M., and J. B. Goodenough. "First-Order Localized-Electron⇆ Collective-Electron Transition in LaCo O 3." *Physical Review* 155.3 (1967): 932.

[19] Tilley, Richard JD. *Defects in solids*. John Wiley & Sons, 2008.

[20] Kamel, Rida. "Synthèse, caractérisation et propriétés catalytiques des oxydes La1-xMxCrO3 (M= Sr et Ce)." *Diss. Thèsedoctorat, UniversitéMentouriCanstantine* (2008).

[21] Dupeux, Michel. *Science des matériaux*. Paris, France: Dunod, 2004.

[22] Boucard, Frédéric. *Modélisation de la diffusion des dopants dans le silicium pour la réalisation de jonctions fines*. Diss. Université Louis Pasteur-Strasbourg I, 2003.

[23] Viciu, Liliana, Vladimir O. Golub, and John B. Wiley. "Structural, thermal and magnetic characterization of the manganese oxyhalide layered perovskite,(MnCl) LaNb2O7." *Journal of Solid State Chemistry* 175.1 (2003): 88-93.

[24] Zhang, Rui, Bei Jiang, and Wenwu Cao. "Elastic, piezoelectric, and dielectric properties of multidomain 0.67 Pb (Mg 1/3 Nb 2/3) O 3–0.33 PbTiO 3 single crystals." *Journal of Applied Physics* 90.7 (2001): 3471-3475.

[25] Sfeir, Joseph. "LaCrO3-based anodes: stability considerations." *Journal of Power Sources* 118.1-2 (2003): 276-285.

[26] Huang, Kevin, and John B. Goodenough. "Solid oxide fuel cell technology: principles, performance and operations." (2009).

[27] Ormerod, R. Mark. "Solid oxide fuel cells." *Chemical Society Reviews* 32.1 (2003): 17-28.

[28] Chehadeh, Mostafa. *A Thermodynamic Analysis of Solid Oxide Fuel Cells*. Diss. Worcester Polytechnic Institute, 2022.

[29] Zhang, R.,Jiang, B. and CAO, W. elastic piezoelectric and dielectric properties of multidomain.0.67PB(Mg1/3Nb2/3)O3-0.33PbTiO3 singlecrystals.journal of applid Physic, 2001.90(7):p3471-3475.

[30] F.A. Kröger ,H.J. Vink, Solid State Physics, Ed. F. Seitz et D. Turnbell, 307, Academic Press, (1956).

[31] Djoudi, Lynda. *Synthèse et propriétés d'oxydes mixtes à base de Lanthane, Aluminium et Nickel*. Diss. Université Mohamed Khider-Biskra, 2016.

[32] Madoui, Nadia. *Synthèse et caractérisation d'oxydes par précipitation des sels précurseurs*. Diss. Université Mohamed Khider-Biskra, 2017.

[33] Guemache, Abderezak. *Synthèse et propriétés électrochimique du système La1-xMxAlO3 M:(Sr, Ca)*. Diss. Université Mohamed Khider-Biskra, 2017.

[34] Aguilar, Gonzalo Galicia. *Etude par spectroscopie d'impédance globale et locale de la corrosion du magnésium et des alliages de magnésium AZ91*. Diss. Université Paris 6-Pierre et Marie Curie, 2006.

Chapter II: Synthesis and characterization methods

Chapter II: Methods of synthesis and characterization

II-1 Methods of preparation of mixed oxides

Materials made of mixed oxides, including as perovskite, spinel, and pyrophore, can be created using a variety of techniques. The ultimate structure of these materials is greatly influenced by the technique of preparation used. The sol-gel method, co-precipitation method, impregnation method, and hydrothermal method are some of the techniques that can be used [1]. The technique of choice is determined by the planned use of the mixed oxide, as it has a direct impact on the morphology and characteristics of the solid that results. These approaches will be identified and contrasted based on factors including specific surface area, calcination temperatures and periods, and the purity of the produced phase in order to ascertain the most favorable way for catalysis[2].

II.1.1 Synthesis by reaction in solid state (ceramic):

The most simplest way to create solid mixed oxide solutions is by solid preparation, which is a simple and economical technique. It is based on an oxide combination reacting at a high temperature.

There are some downsides to the solid route synthesis process. One of the primary problems is that the reaction is frequently insufficient, which leads to an insufficient conversion of the raw materials into the intended output. Furthermore, the calcined powder produced by this process frequently has an uneven composition and lacks consistency throughout the substance [3].

The steps listed below can be used to create perovskite utilizing the solid route synthesis method:

a) Raw materials

The components of mixed oxide materials can include oxides, carbonates, nitrates, and other substances. For these materials, the optimal powder has tiny grains with a narrow size distribution, usually around 1µm . The powder's purity and any additional ingredients are strictly regulated. However, determining the reactivity of the powdered base raw materials can be difficult. The substance's

Its thermal history and response to other components are important elements that profoundly affect its properties **[4].**

b) Mixing and grinding

The manufacture of structured solid perovskites depends on this step. A consistent distribution of precursors is attained at this phase. The weights of the powders are determined by the stoichiometric ratios that the reaction equation predicts.

c) Calcination

Materials are subjected to a heat cycle, frequently in a controlled atmosphere, in order to promote the desired phase development. The materials go through phase reactions through diffusion processes, which leads to the production of the desired phase. Carbon dioxide, oxygen dioxide, and even water vapor may all be emitted during this reaction.

d) Regrinding

The powder is further treated to reduce grain size, improve homogeneity, and boost reactivity after the heat treatment. This is accomplished by recreating the powder using appropriate techniques. To produce the appropriate phases, the powder is subsequently heated at a high temperature **[5].**

This straightforward method does, however, have a number of drawbacks despite being widely used **[6, 7].**

- Low reaction rates in solid states; these rates rely on the thermal cycle employed (heating rate and annealing period). High temperatures are applied, which uses a lot of energy.
- Because of the emergence of a liquid phase during the crystallization of grains under magnification, the grain size is too large.
- The final product's composition is not uniform, with the mean composition deviating from the anticipated composition.

- Extrinsic impurities result from the nacelle of the crusher being contaminated, a furnace being contaminated by volatile oxides (Pb, Bi, Li, etc.), or an interaction with ambient moisture.

II.1.2. Wet (liquid) synthesis

II.1.2.1 Sol-Gel Method

gel procedure. A "sol" is basically -solution gel" is a term used to describe the-Sol" a colloidal suspension containing oligomers that are smaller than nanometers. This sol can then go through reactions to create the "gel," an infinitely viscous network. The s to polymerize molecular precursors in a gel method i-basic idea behind the sol solution to produce an oxide network. The transition from a liquid to a solid phase involves a number of chemical processes, including polymerization, condensation, takes place at room temperature, it and hydrolysis. Because this procedure frequently is also referred to as "soft chemistry." Densifying the material and obtaining the requisite characteristics for certain applications require additional heat treatment. gel process is -monoliths, the sol When creating different oxide structures, such as .versatile

II.1.2.2 Co-precipitation

Chemically, this approach for making oxides (perovskites) is the earliest. simultaneous co-recipitation of the precursors of an amorphous molecule that is rather homogeneous. Acetate, chloride, and nitrate are combined in water with the precursors for sites A and B of the perovskite structure. Following the intermediate steps of settling, rinsing, and filtration, all species are then precipitated at basic pH as oxalate or hydroxide. The precipitate is then washed to break up agglomerates. The amorphous precipitate is dried, then calcined to produce the perovskite phase. This process enables the use of very small crystals. Controlling the velocities of the four kinetic stages that intervene in the coprecipitation of a solid is required in order to regulate the morphology, size, and distribution of particle sizes at the end of the process. They are as follows:

- A condensed precursor is produced.
- Bacteria are created through condensation.
- includes the growth of microorganisms through condensation.
- The particles' aging.

By adjusting several factors, such as pH, concentration, and temperature, it is possible to regulate the kinetics of the synthesis processes. The reaction rate and ultimate characteristics of the perovskite material are greatly influenced by these parameters **[9, 10].**

II.1.3 . Comparison between these methods

Table II.1. proposes the main advantages and disadvantages of these methods

presented above.

Table II.1: Comparative study of the different synthesis methods**[9].**

Méthode	Avantages	Inconvénients
Voie solide	Stabilité thermique	Activité plus faible
Sol gel	Flexible, dispersion homogène, technologie mature	Solvant, résidus carbonés
Co-précipitation	Fortes surfaces, faible contamination C, stabilité thermique	Solvants, méthode dépendant de la pérovskite

II.2.Characterization methods:

Active Pharmaceutical Ingredients (APIs) are studied and characterized in their solid-state forms using a variety of analytical techniques. These methods offer useful details that help in comprehending the characteristics and behavior of the APIs. We will concentrate on how each technique is used explicitly in the context of solid-state transformations rather of going into depth about each technique or the underlying principles, which are easily available in literature and outside the scope of this study**[11]**

.

II.2.1. Thermal analysis:

This extremely sensitive technique can be used with small sample quantities, typically 10 to 25 mg, and permits the detection of minute thermal events. A controlled temperature increase can cause a variety of events, such as the release of various types of water, breakdown, or structural changes. Differential thermal analysis (DTA) and thermogravimetric analysis (TGA) are typically utilized in equipment for this purpose **[12]**.

Figure II.1: Thermal analysis apparatus ATG-ATD << Schimadzu >>.**[13]**

II.2.1.1 Thermogravimetric Analysis (TGA):

A thermal technique called thermogravimetric analysis (ATG) examines changes in sample mass under isothermal circumstances or ramped heating at a predetermined rate. Weight loss at lower temperatures is often attributed to solvent evaporation when the drug's melting point is not achieved. When compared to solvent incorporated in the crystal structure, the loss of adsorbed or absorbed moisture or solvent vapor is

frequently observed to occur gradually. The amount or percentage of weight lost at particular temperatures can be calculated by examining the weight loss profiles.

Additionally, the stoichiometric relationship can be established by taking into account the molecular weights of the medication and the lost solvent **[11].**

Figure II.2 : apparatus TG: 70/217Thristor-Power supplylinse **[14]**

II.2.1.2. Differential Thermal Analysis (DTA):

Using a technique called differential thermal analysis (DTA), it is possible to determine the temperature difference between a reference material and a sample over time or at a certain temperature. The ability to distinguish between exothermic and

endothermic reactions, each shown by a peak on the DTA curve, is made possible by this temperature difference. These distinctive characteristics are frequently seen in substances. Under a specific atmosphere, the system's temperature can be set and regulated. The temperature variation happens gradually to guarantee that equilibrium is reached at every moment **[12].**

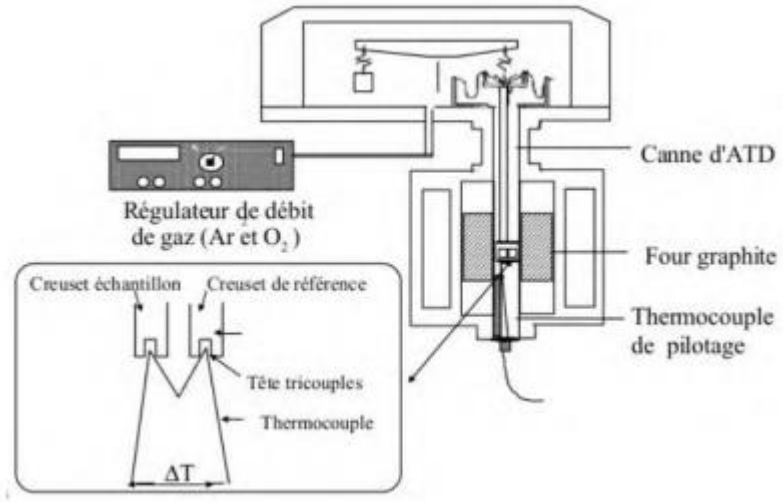

Figure II.3: Operating principle of the ATD system **[10]**

II.2.2 X-ray Diffraction - Powder Method

An approach called X-ray powder diffraction (XRPD) is used to create distinctive X-ray diffraction patterns that correlate to individual drug's crystalline arrangements. This method can be used to identify things, especially to differentiate between several polymorphs. Peak positions seen in the diffraction pattern will shift whenever there is a change in the crystal structure. Additionally, by tracking changes in the intensity of peaks that are particular to each form over time, XRPD can be used to quantitatively calculate the relative proportions of two forms during a transformation process. Transformations brought on by changes in humidity or temperature can be investigated using an X-ray diffractometer with a controlled temperature chamber. An amorphous substance won't produce the XRPD pattern.In the event of an amorphous substance, the XRPD pattern will show broad humps instead of distinct peaks, known as an amorphous halo. Peaks appearing on the diffraction pattern are proof that an amorphous substance has crystallized. Although the amorphous halo lacks information about specific peaks, it does reveal the short-range organization present in the substance. The degree of short-

range order can be assessed using high-energy X-ray sources and pair-distribution-function analyses, and it is occasionally possible to match it to the crystal structure with the closest arrangement **[11]**.

II.2.2.1. Principle of the method:

An essential method for figuring out the structures of crystalline materials is X-ray diffraction. It offers useful details regarding the compositional analyses (qualitative and quantitative), texture, internal stresses, atom distribution within the unit cell, lattice parameters, and crystal symmetry. The composition of the material can be ascertained by contrasting the locations and intensities of the observed diffraction lines.

In X-ray diffraction, the crystal's atomic planes interact with the incident X-ray beam to produce constructive interference. The incident beam's angle of incidence with respect to the crystal planes must be such that the reflected waves are in phase and interact positively in order to quantify diffraction. The given figure serves as an illustration of this. The Bragg equation provides a description of the circumstances that lead to this constructive interference**[15].**

$$n\lambda = 2d_{hkl}\sin\theta_{hkl}$$

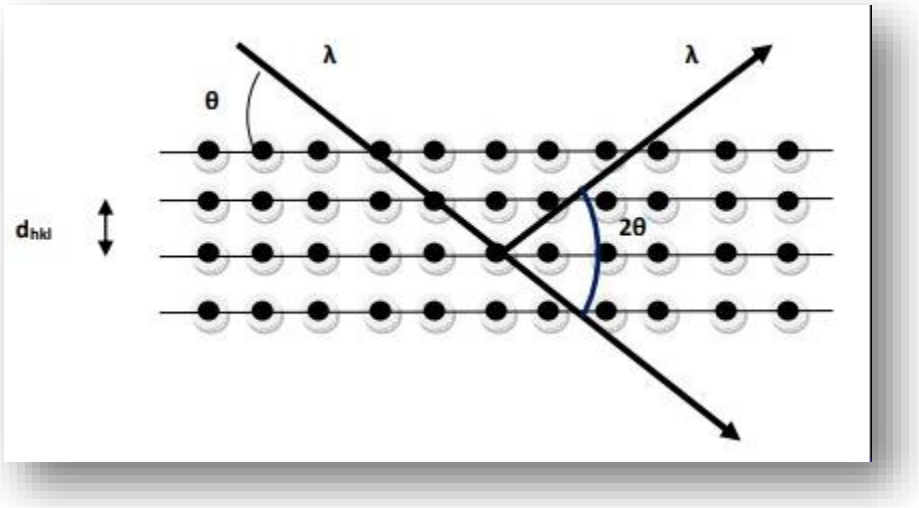

Figure II.4: Family of crystal planes in deBragg condition

n: the order of diffraction (whole number)

λ: the wavelength of the incident beam

θ_{hkl}: the angle between the incident beam and the diffracting planes of Miller indices (hkl)

d_{hkl}: represents the characteristic reticular distance of the atomic planes (hkl)

II.2.2.2 Structure refinement

Following the X diffraction pattern recording, carry out the following steps:

- Starting with the dhkl that corresponds to the greatest intensities, the observed values are compared to the values listed in the ASTM file (American Society for Testing and Material) or published in the papers.

- Defining the planes to which each reflection belongs is the indexing process for the diffraction diagram. Thus, a list of observed dhkl values and their corresponding intensities is generated.

- Rietveld technique refinement of the overall profile..

II.2.3 Fourier Transform Infrared Spectroscopy (FTIR)

By giving distinct spectral fingerprints of the samples, FTIR (Fourier Transform Infrared Spectroscopy) is a qualitative analytical method used to examine surface changes and functionalization. By identifying absorption or emission peaks that correspond to the vibrational frequencies of atomic bonds inside the material, it can measure the infrared spectrum. The spectrum is typically captured between 400 and 4000 cm^{-1}, which matches to the samples' chemical fingerprint.

FTIR can be combined with other methods, such as attenuated total reflectance (ATR), to create FTIR-ATR, which broadens the applicability of FTIR. Using this method, surfaces with a few micron-sized (0.5–3 m) absorption or emission spectra can be measured. The evanescent wave produced by an internal reflection element serves as the foundation for ATR.

Other cutting-edge methods have also been widely used for material characterisation in addition to FTIR-ATR, including FTIR-microscopy, FTIR-photoacoustic spectroscopy (FTIR-PAS), FTIR-polarized optical microscopy, and

nano-FTIR spectroscopy. These methods offer insightful information about the make-up, structure, and characteristics of materials at various scales**[16]**.

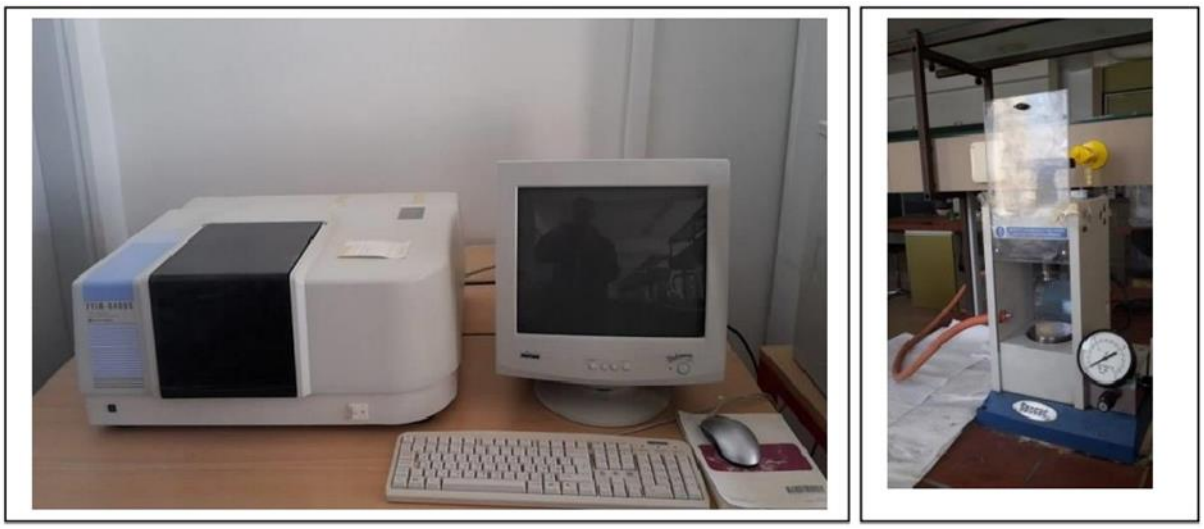

Figure II.5 : Spectromètre à transformée de Fourier (FTIR) Shimadzu 8400 s**[17].**

II.2.4 Analysis of particle size curves

Granulometry is a method for evaluating the particle size distribution of powders quantitatively. The interaction of particles and laser radiation is essential to the measurement procedure. To guarantee appropriate dispersion, the granules are first dissolved in a solution and exposed to ultrasound. The dispersed particles then travel through a sampling module outfitted with an ultrasonic probe as a small amount of the diluted solution is then added to a measuring tank. A laser beam passes through an optical cell that contains a suspension of particles. For accurate measurements, it is vital to have a thorough understanding of the optical characteristics of both the powders and the solvents. A laser particle size analyzer from the Malvern Mastersizer series (2000/3000) was utilized for this analysis. This instrument has a wide coverage of particle size ranges since it can measure particles with sizes ranging from 0.3 m to 300 m. The analyzer offers useful data, including the size distribution's shape and defining diameters like the mean and median diameters (d50) . The size distribution of the powder particles can be described and understood using these factors**[18].**

Figure II.6: granulomere laser Malvern Mastersizer 2000/3000 **[18].**

II.2.5 Scanning Electron Microscopy (SEM)

The scanning electron microscope (SEM) is an electron microscopy method that can create images of a sample's surface and is based on the interaction of electrons with matter **[19].**

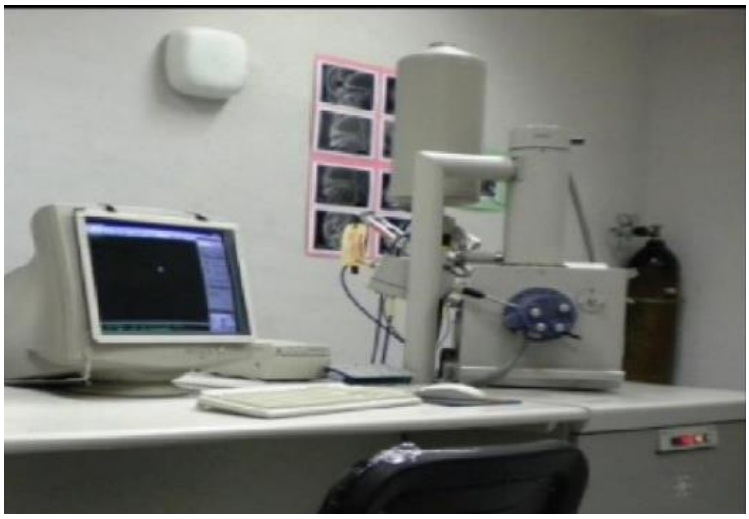

Figure II.7: SEM Block Diagram**[20],[10].**

II.2.5.1 Principle

The basic idea behind scanning electron microscopy (SEM) is to utilize an electron beam to scan the sample's surface before analyzing it. Based on the groundbreaking work done in the 1930s by Max Knoll and Manfred von Ardenne, this method was created. The sample's surface is impacted by the electron beam, and the resultant particles are picked up by a variety of detectors to create a three-dimensional image of the surface.

During the process of de-excitation, X-ray photons are released as a result of the excitation caused by the incident electrons' interactions with the material's atoms. The incident electron energy, the sample's average atomic number, and the energy of the originally ionized level are a few examples of the variables that affect the volume of X-ray photon emission, which is typically on the order of μm3 **[20].**

Referances

[1] Nikonov, A. V., et al. "A brief review of conductivity and thermal expansion of perovskite-related oxides for SOFC cathode." *Eurasian Journal of Physics and Functional Materials* 2.3 (2018): 274-292.

[2] Boumaza, S., et al. "Photoelectrochemical study of La 2 NiO 4 synthesized using citrate sol gel method—application for hydrogen photo-production." *Journal of Solid State Electrochemistry* 24 (2020): 329-337.

[3] Guemache, Abderezak. *Synthèse et propriétés électrochimique du système La1-xMxAlO3 M:(Sr, Ca)*. Diss. Université Mohamed Khider-Biskra, 2017.

[4] Cristian PERCA << Structure cristalline et magnétique de pérovskites RBaMn2O6-ä (où a = 0 et 0,5) >> thèse doctorat, Université Paris XI (2005).

[5] Abdelhadi Aydi << Elaboration et caractérisation diélectriques de céramiques ferroélectriques et/ou relaxeur de formule MSnO3-NaNbO3 (M= Ba, Ca) >> thèse doctorat, Université Bordeaux 1 (2005).

[6] L .Smart et E.Moore, Introduction à la Chimie du Solide, Masson Paris (1997).

[7] C. Boudaren, Thèse de Doctorat, Constantine, Algérie (2002).

[8] A.J. Bosman, E.E. Havinga, « Temperature dependence of dielectric constants of cubic ionic compounds », Physical Review 129 (1963) 1593-1600.

[9] A. Gil, L.M. Gandia, S.A. Korili. Appl.Catal. A 274 (2004) 229.

[10] BENAICHA, Abdelhakim. Synthèse et propriétés des oxydes LaFe1-xCuxO3. Diss. Université Mohamed Khider-Biskra, 2018.

[11] Mastai, Yitzhak, ed. *Advanced Topics in Crystallization*. BoD–Books on Demand, 2015.

[12] Abdellah, Mr BAHMANI. "Synthèse, caractérisation et propriétés électriques d'oxydes mixtes dans les systèmes Sr-Ca-Bi-O et Sr-Sn-Ti-O." *en ligne]. Thèse de doctorat, université des sciences et de la technologie, Oran, 2012.[consulté le 24/05/2022]. Disponible à l'adresse http://www. univ-usto. dz/theses_en_ligne/doc_num. php? explnum_id* 870 (2012).

[13] Fodil, Hanane. Etude physicochimique des oxydes mixtesBaFe1-x AlxO3. Diss. Université Mohamed Khider-Biskra, 2016.

[14] Djoudi, Lynda. Synthèse et propriétés d'oxydes mixtes à base de Lanthane, Aluminium et Nickel. Diss. Université Mohamed Khider-Biskra, 2016.

[15] BENOIT LEVASSEUR, Effet des cations A et B dans la structure perovskite ABO3 sur la catalyse de l'oxydation du methanol. Thèse (2009) (Université LAVAL QUEBEC

[16] Pandey, Lalit M., and Abshar Hasan, eds. *Nanoscale Engineering of Biomaterials: Properties and Applications*. Springer, 2022.

[17] Lavat, A. E., & Baran, E. J. (2003). IR-spectroscopic characterization of A 2 BB′ O 6

perovskites. Vibrational spectroscopy, 32(2), 167-174.

[18] Diafi, Malika. *Synthèse et propriétés physiques d'oxyde mixtes à base de lanthane calcium et aluminium*. Diss. Universite Mohamed Khider-Biskra, 2013.

[19] C. Ayral, « Elimination de polluants aromatiques par oxydation catalytique sur charbon actif », thèse de doctorat ; Université de Toulouse, 2009.

[20] Guemache, Abderezak. *Synthèse et propriétés électrochimique du système La1-xMxAlO3 M:(Sr, Ca)*. Diss. Université Mohamed Khider-Biskra, 2017.

III.Chapter: Synthesis and characterization of the oxide $LaFeO_3$ and discussion of the results bibliographically

Chapter III: Synthesis and characterization of LaFeO3 oxide and discussion of the biblio results graphically

III.1 Introduction:

In this chapter, we compared the different ways of synthesis (sol-gel, hydrothermal, solid state) for the mixed oxide of perovskite structure based on lanthanum LaFeO3:

1. using the sol-gel process to create LaFeO3
2. LaFeO3 is created by a hydrothermal process in
3. Solid state technique of LaFeO3 synthesis

thermal analyses, including thermogravimetric and differential thermal analyses, Fourier transform infrared (FT-IR). SEM, and rays (DRX).

The utilization of LaFeO3 in each technique of synthesis was then contrasted.

III.2 Preparation of LaFeO3 Oxide

III.2.1 The Sol-Gel method

The sol-gel combustion technique was used to create LaFeO3 particles. First, using a magnetic stirrer, lanthanum nitrate hexahydrate and iron nitrate nonahydrate were dissolved in distilled water in stoichiometric quantities (1:1 molar ratio). Citric acid and ethylene glycol were then added to the precursor solution after the metal salts had completely dissolved in the solution. The total molar amount of metal nitrates in the solution was equal to the molar amount of citric acid and 5 mL of ethylene glycol. The total molar amount of metal nitrates in the solution was equivalent to the molar amount of citric acid. To create the gel, this solution was heated to 70–80 °C on a heating plate while being stirred for a number of hours using a magnetic stirrer. To create dry particles known as xerogel powders, the gel formation was quickly placed into an electrical oven set at 110 °C for 5 hours.In a muffle furnace, these powders were crushed and calcined at 400, 450, and 500 °C for five hours. The chosen sample was sintered

at 800, 900, and 1000 °C for 4 hours in accordance with XRD analysis, which indicates that 450 °C is the ideal calcined temperature [1,2].

III.2.2 hydrothermal method

The hydrothermal process was used to create LaFeO3 microspheres, using $La(NO_3)_36H_2O$, $Fe(NO_3)_36H_2O$, and $C_6H_8O_7H_2O$ as the foundational components. In a typical synthesis, 30 ml of double-distilled water was mixed magnetically while a

stoichiometric amount of lanthanum nitrate hexahydrate and ferric nitrate nonahydrate were dissolved. A suitable amount of citric acid monohydrate was added to the mixture, with the molar ratio of citric acid to metal nitrates in the solution being the same. The resulting reaction mixture was put into a 40 cc Teflon-lined stainless autoclave, sealed, and allowed to continue reacting for a range of periods, from 6 to 24 hours, at 180 °C. The autoclave was then allowed to naturally cool to ambient temperature after the reaction.The resultant precipitate, which had a light green hue, was centrifuged to separate it, and it was then repeatedly rinsed with deionized water and anhydrous ethanol. The precipitate was next dried in ambient air for two hours at 80 °C before being calcined for two hours at 800 °C. LaFeO3 powder was produced as a result of these processes [3,4].

III.2.3 Solid state method

LaFeO3 nanoparticles were created via mechanical ball milling as part of a solid-state synthesis process, and their usefulness in the detection of dopamine was investigated. While other techniques, including hydrothermal, microwave-assisted, and wet chemical procedures, have been reported for the synthesis of LaFeO3, the ball milling process has benefits in terms of ease of use and enhanced reactant mixing, producing smaller particles with more surface area. using electrocatalysis There are only a few reports on the detection of dopamine using LaFeO3, and the activity of

dopamine oxidation was investigated using a LaFeO3 modified electrode, highlighting the role of Fe in enhancing the catalytic activity. The detection of dopamine was carried out using a pulse voltammetric technique to assess the selectivity and reliability of the proposed sensor for human biological samples. The results of this study provide valuable insight. The selectivity and dependability of the suggested sensor were assessed, notably in the setting of human biological samples[5,6].

III.3 LaFeO3 powder characterization methods

III.3.1 X-ray diffraction analysis

- **Sol-Gel method**

Works by Mya Theingi , Kay Thi Tun , Nwe Nwe Aung [1,2]

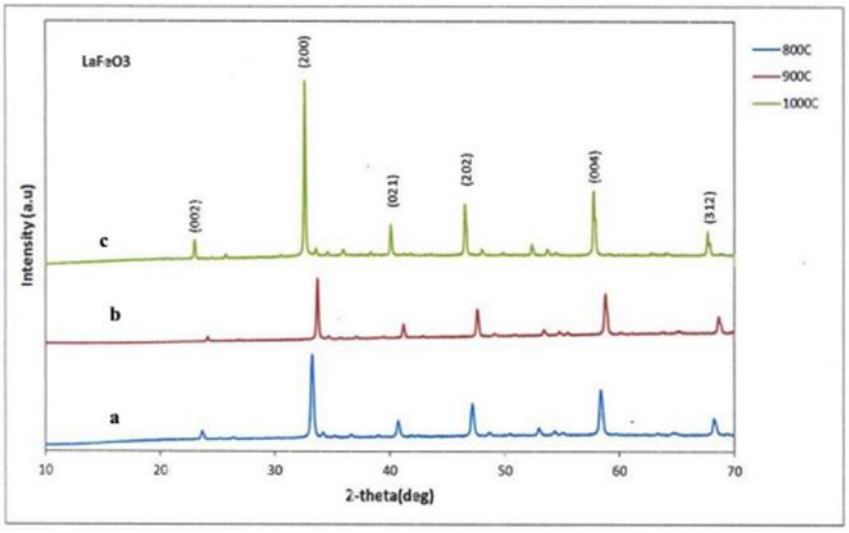

Figure III.1. XRD patterns of $LaFeO_3$ samples sintered at (a) 800 ˚C, (b) 900 °C and (c) 1000 ˚C

Figure III.1 shows the X-ray diffraction (XRD) patterns of LaFeO3 particles sintered at 800, 900, and 1000 °C. According to the XRD investigation, high-temperature sintering caused the crystal structure to shift to an orthorhombic phase. The Pbmn space group was visible in the LaFeO3 particles. In addition, the

samples' crystallite sizes sintered at 800, 900, and 1000 °C were identified. The sample sintered at 800 °C had a crystallite size of 51.27 nm, the sample sintered at 900 °C had a crystallite size of 49.75 nm, and the sample sintered at 1000 °C had a crystallite size of 66.70 nm. Following the corresponding sintering temperatures, these numbers represent the average size of the crystalline domains in the LaFeO3 particles.

❖ hydrothermal method

works by S. Thirumalairajan , K. Girija , I. Ganesh , D. Mangalaraj , C. Viswanathan , A. Balamurugan , N. Ponpandian [3,4]

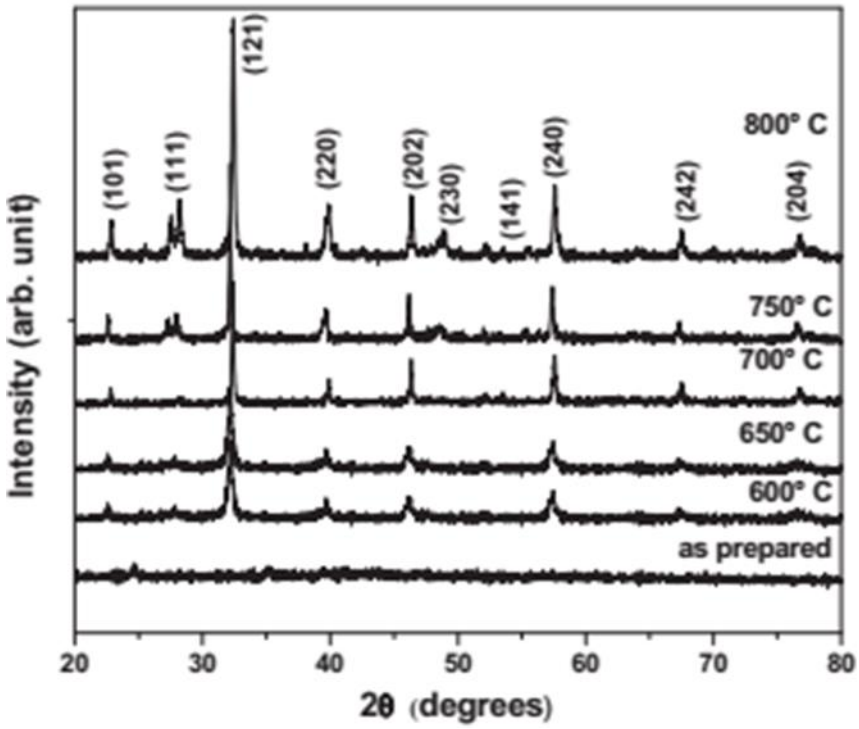

Figure.III.2. XRD pattern of $LaFeO_3$ nanoparticles for different calcination temperature.

Figure III.2 demonstrates the X-ray diffraction (XRD) patterns of LaFeO3 samples that were created as-is and those that were treated to various calcination temperatures. The sample is amorphous in form and has no clear crystalline features; it

is distinguished by large continuum peaks. This shows that just a few distinctive peaks of low intensity for LaFeO3 were present in the XRD pattern at 600 and 650 °C, indicating that the transformation from the amorphous phase to crystalline LaFeO3 was not totally complete at those temperatures. LaFeO3 crystallization begins to show up more clearly as the calcination temperature rises, albeit with low intensity peaks at 700 °C and 750 °C. On the other hand, well-crystallized orthorhombic perovskite-type LaFeO3 (matching to JCPDS 37-1493) is produced at 800 °C. When compared to samples that were calcined at lower temperatures, the samples have comparatively excellent crystalline quality, as evidenced by the crisp and narrow

diffraction peaks found at 800 °C. The ferocity of The growth and better crystallinity of LaFeO3 microspheres are shown by an increase in the diffraction peaks with an increase in the calcination temperature.

❖ Solid state method

works by Thiruvenkadam Vijayaraghavan, Ramanathan Sivasubramanian, Shamima Hussain, and Anuradha Ashok[5,6]

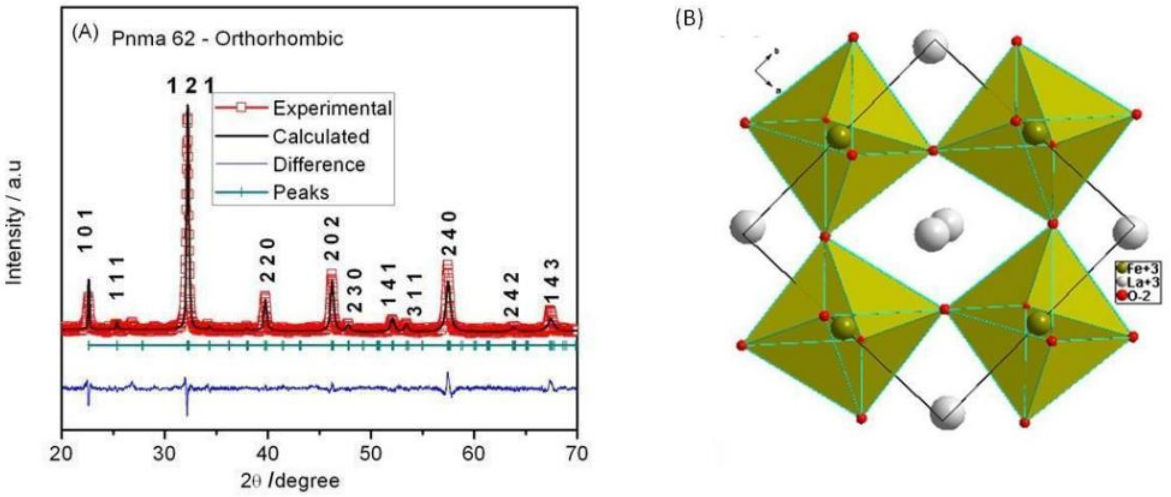

Figure.III. 3. A) XRD pattern of $LaFeO_3$ nanoparticles and B) Pictorial representation of unit cell of $LaFeO_3$.

The diffractogram shows that the LaFeO3 material has an orthorhombic crystal structure with a primitive lattice, belonging to the space group Pnma (62) based on the

reported data from the crystal structure database JCPDS No. 37-1493 **(Figure. III. 3.** A). **Table III.1** has more details about the crystal structure. It is discovered that the computed cell parameters agree with the theoretical values discovered through Rietveld analysis. This demonstrates that the LaFeO3 sample is highly crystalline and that there are no secondary peaks in the XRD pattern that would suggest unreacted materials, contaminants, or side products, hence demonstrating the phase purity of LaFeO3. Diamond software was used to produce the LaFeO3 unit cell, which is depicted in Figure 3B. The slanted Fe octahedra inside the unit cell are thought to be responsible for the perovskite LaFeO3's orthorhombic symmetry. The Debye-Scherrer

formula, which takes the X-ray wavelength, full width half maximum, and diffraction angle into account, calculates the average crystallite size as being 31.27 nm.

Table.III.1. Lattice parameters of $LaFeO_3$

Sample	Crystal unit	Centering	Space group	Crystallite size (nm)	Cell parameters (Theoretical)	Cell parameter (Calculated)
LaFeO3	Orthorhombic	Primitive	Pnma (62)	31.27	a-5.5663 b-7.8544 c-5.5533	a-5.5392 b-7.8573 c-5.5584

III.3.2 Infrared Spectroscopy Analysis

❖ Sol-Gel method

Works by Mya Theingi , Kay Thi Tun , Nwe Nwe Aung [1,2]

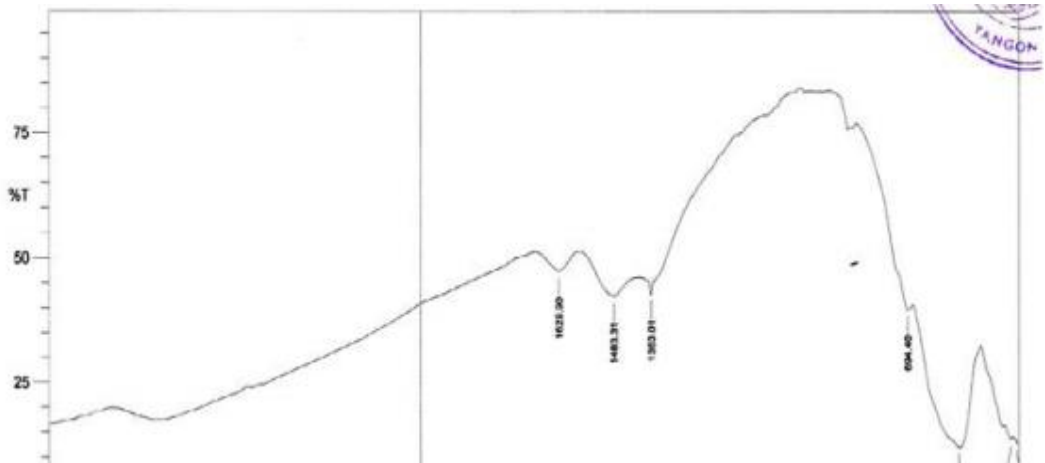

Figure III.4. FTIR spectrum of $LaFeO_3$ nanocrystalline particle calcined at 450 °C

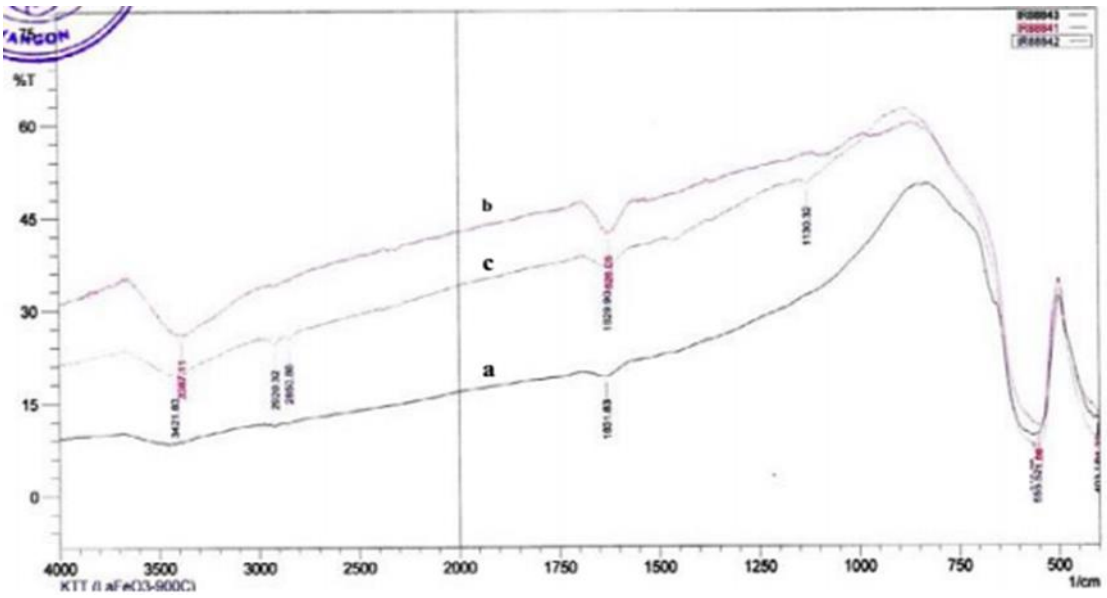

Figure III.5. FTIR spectra of $LaFeO_3$ nanocrystalline particles sintered at (a) 800 ˚C, (b) 900 ˚C and (c) 1000 ˚C

Figure III.4 shows the LaFeO3 particle's FTIR spectrum after it has been produced and calcined at 450 °C. The O-H stretching vibration is represented by absorption bands in the spectra that fall between the wavelengths of 3400 and 3000 cm1. A band between 1400 and 1500 cm1 also reveals the C-O stretching vibration coming from lingering carbon. The band at 800-900 cm1 is corresponding to the residual carbon-induced C-H bending vibration. In addition, the bands between 400

and 750 cm 1 are the stretching vibration of metal-oxygen bonds. In**Figures III.5(a), 5(b)**, and **5(c)**, The LaFeO3 particles sintered at 800, 900, and 1000 °C, respectively, are shown in their FTIR spectra. These spectra show stronger and more pronounced bands between 400 and 750 cm-1. This is explained by the elevated vibrations of metal-oxygen stretching and the absence of carbon residues brought on by the high-temperature processing. The numbers provided in the literature match up with the FTIR measurements obtained for the manufactured LaFeO3 samples.

❖ hydrothermal method

works by S. Thirumalairajan , K. Girija , I. Ganesh , D. Mangalaraj , C. Viswanathan , A. Balamurugan , N. Ponpandian [3,4]

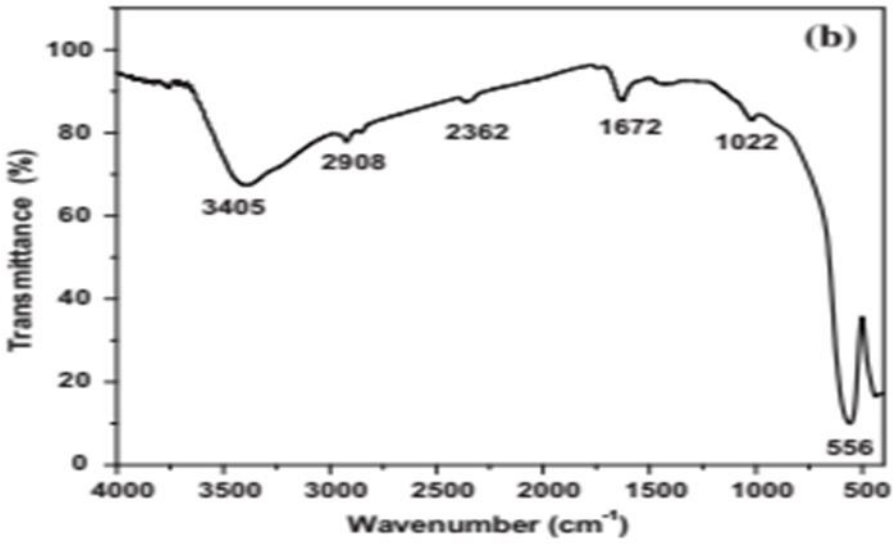

Figure III.6. FTIR spectrum of 12 h $LaFeO_3$ nanoaprticles**.**

Figure III.6 shows the LaFeO3 FTIR spectrum after a 12-hour period. The spectrum shows a number of bands, each of which corresponds to a separate functional group and vibration. The H-O bending mode of absorbed water or hydroxyl groups is characterized by the band seen at 3405 cm1. A band that represents the physically absorbed CO2 is visible at 2908 cm1. Two more bands, which result from the

symmetric and asymmetric stretching of the carboxyl group, are shown at 2362 and 1627 cm1. The primary vibration of the CO32- group is represented by a smaller peak at 1022 cm1, which denotes the presence of La-carbonate species on the surface of LaFeO3. It implies exposure to the surrounding atmosphere and points to the presence of carbonates that the XRD study did not pick up on. Additionally, the Fe-O stretching vibration, a feature of the octahedral FeO6 group present in LaFeO3, is credited with creating the band at 556 cm1. The spectrum did not, however, show any standout typical peaks of surface-adsorbed oxygen species.

❖ Solid state method

works by Thiruvenkadam Vijayaraghavan, Ramanathan Sivasubramanian, Shamima Hussain, and Anuradha Ashok [5,6]

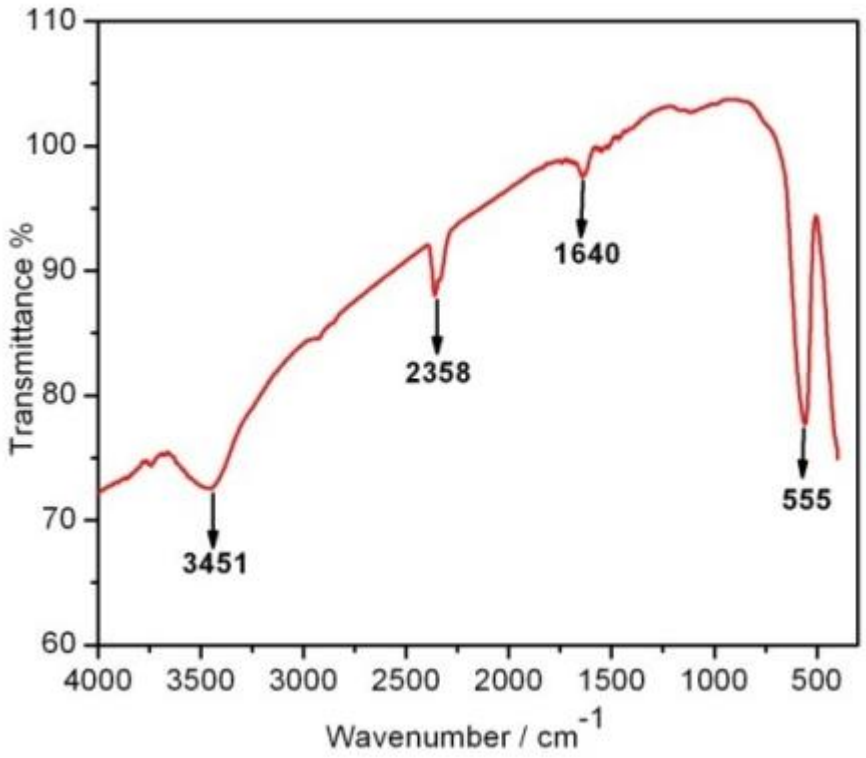

Figure III.7: FTIR spectra of $LaFeO_3$ nanoparticles.

Figure III.7. to the stretching vibration and bending vibration of OH groups,

respectively, in the FTIR spectra of LaFeO3 nanoparticles. Due to the atmospheric carbon dioxide's adsorption and the measurement's lack of an atmospheric adjustment, the symmetric stretching of the carboxyl C=O bond was seen at 2358 cm-1. The octahedral FeO6 present in the LaFeO3 is confirmed by the sharper, more intense peak seen at 555 cm-1 caused by the presence of stretching vibration of FeO.

III.3.3 Thermal analysis (T.A.G – T.A.D) of the precursor

❖ **Sol-Gel method**

Works by Mya Theingi , Kay Thi Tun , Nwe Nwe Aung [1,2]

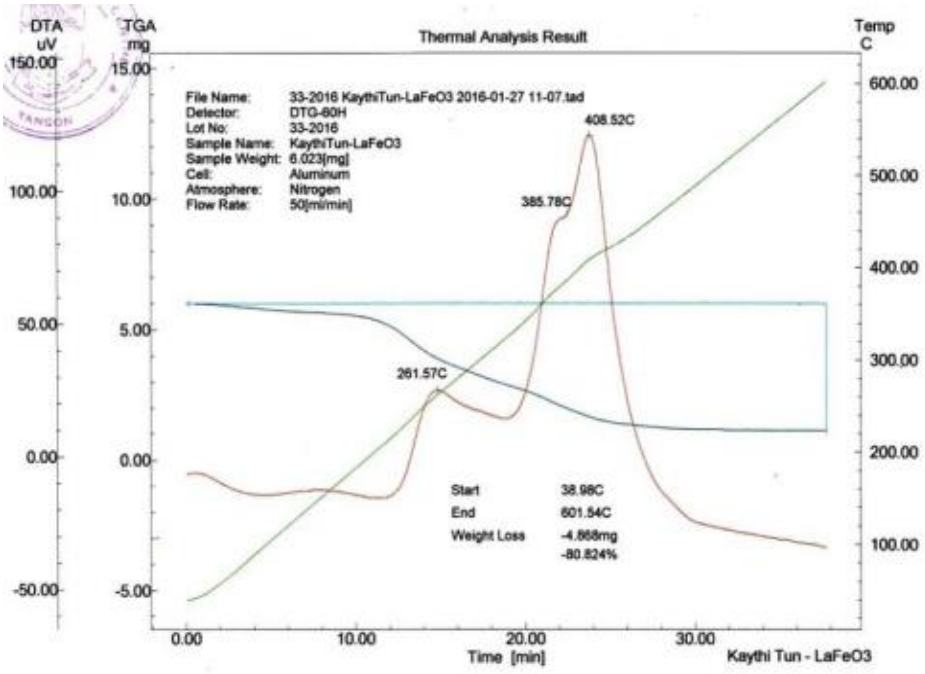

Figure III.8. TG-DTA curves of the thermal decomposition of $LaFeO_3$ xero-gel powder

LaFeO3 xerogel powder's TG-DTA curves show a number of thermal changes.

Three distinct exothermic peaks, measuring 261, 365, and 408 °C, are among them. While peaks at 231 °C, 358 °C, and 544 °C, respectively, show the disintegration of organic molecules, residual nitrates, and the production of the desirable LaFeO3 perovskite phase, they correspond to the loss of adsorbed water at roughly 100 °C.

❖ hydrothermal method

works by S. Thirumalairajan , K. Girija , I. Ganesh , D. Mangalaraj , C. Viswanathan , A. Balamurugan , N. Ponpandian [3,4]

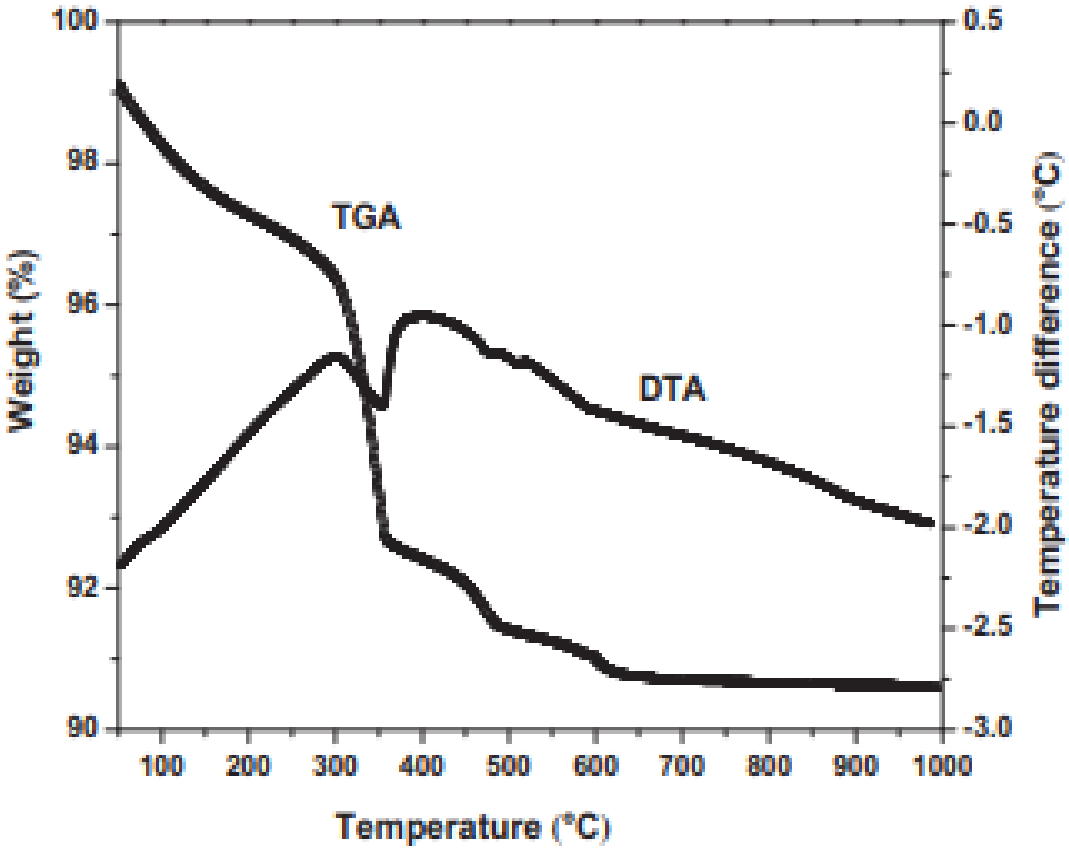

Figure III.9: TG/DTA analysis of $LaFeO_3$ for 12 h.

Between 50 and 295 °C, the TG curve shows a weight loss of 2.2%, which corresponds to the desorption of physically adsorbed water and the breakdown of citric acid. The exothermic peak seen at 300 °C in the DTA curve lends weight to this. Additionally, the broad exothermic peak in the DTA curve at about 365 °C suggests that the progressive weight loss of 4.1% between 300 and 360 °C is caused by the breakdown of nitrates. The total breakdown of oxycarbonates between 435 and 490 °C also results in a small weight loss of 1.8%. LaFeO3 may have crystallized gradually, according to an exothermic peak seen at 550 °C. Overall, the hypothesized chemical formula LaFeO3 is strongly supported by the TG/DTA curves. (For a reference, see **Figure** III.**9**).

❖ **Solid state method**

works by Thiruvenkadam Vijayaraghavan, Ramanathan Sivasubramanian,Shamima Hussain, and Anuradha Ashok[5,6]

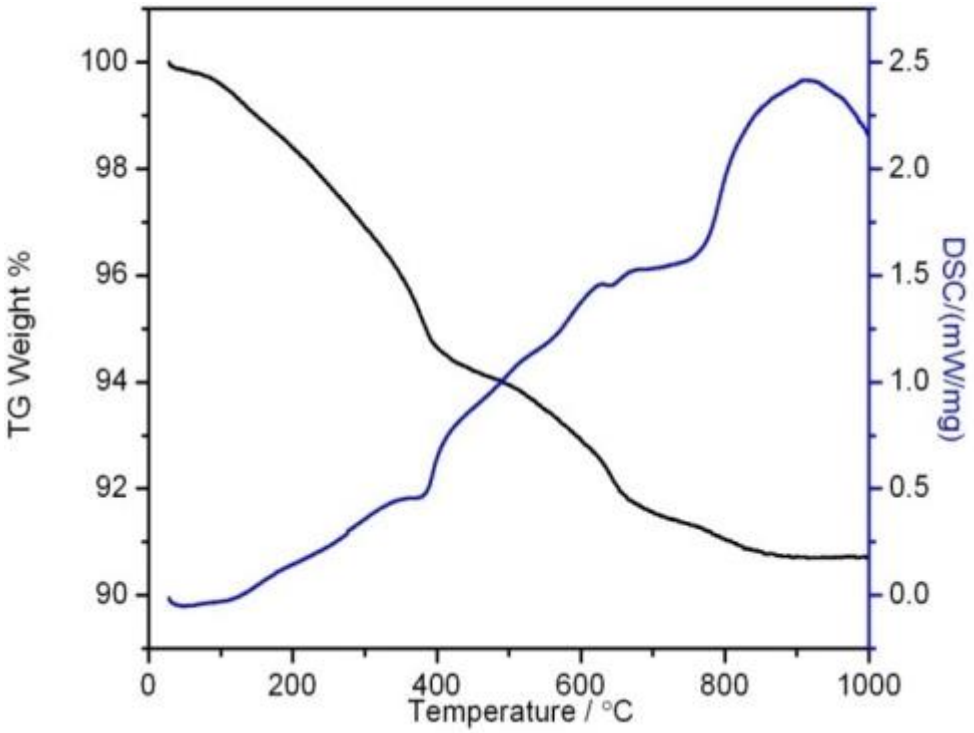

Figure III.10: TGA/DSC curves of ball milled precursors of $LaFeO_3$

Figure III.10 depicts the TGA/DSC curves produced from LaFeO3 precursors that were ball-milled. The measurements were made using a heating rate of 208°C min-

1 and a temperature range of 268°C to 10008°C. The dehydration of LaFeO3 is what caused the initial weight loss of 4.3% at about 3688 degrees Celsius. The exothermic peak at 4008°C in the DSC curve further supports this. Another 2.4% weight loss occurred between 3688 and 6888 degrees Celsius, demonstrating the transformation of LaOOH into La2O3. The DSC curve at 6208°C shows a modest peak that clearly shows this transition. A further weight decrease of 0.9% was also recorded. The breakdown of unreacted species occurs in the temperature range of 6908 °C to 8408 °C. No discernible weight loss was seen above 8408°C, indicating that the material did not undergo any phase or structural changes. In order to obtain LaFeO3 with good phase purity and crystallinity, a calcination temperature of 9008°C was chosen.

III.3.4 .Scanning Electron Microscopy (SEM) analysis:

❖ **Sol-Gel method**

Works by Mya Theingi , Kay Thi Tun , Nwe Nwe Aung [1,2]

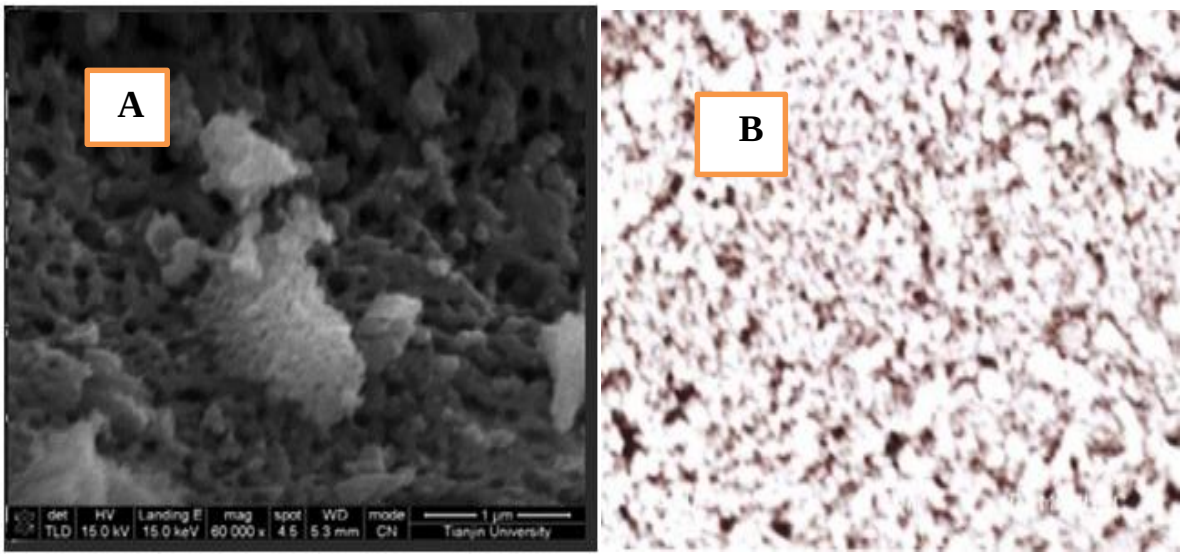

Figure III.11: SEM micrographs of $LaFeO_3$ nanocrystalline particles calcined at 450 °C (a), and micrographs $LaFeO_3$ nanocrystalline particles sintered at 900 °C (b).

Figure III.11 displays the SEM pictures of particles that were calcined at 450 and 900 degrees Celsius. LaFeO3 particles that have been calcined at 450°C have surfaces that

are porous and have agglomerations on them. The LaFeO3 nanoparticles sintered at 900 °C, on the other hand, likewise have a porous structure, but the particles have a compact and uniform distribution.

❖ hydrothermal method

works by S. Thirumalairajan , K. Girija , I. Ganesh , D. Mangalaraj , C. Viswanathan , A. Balamurugan , N. Ponpandian [3,4]

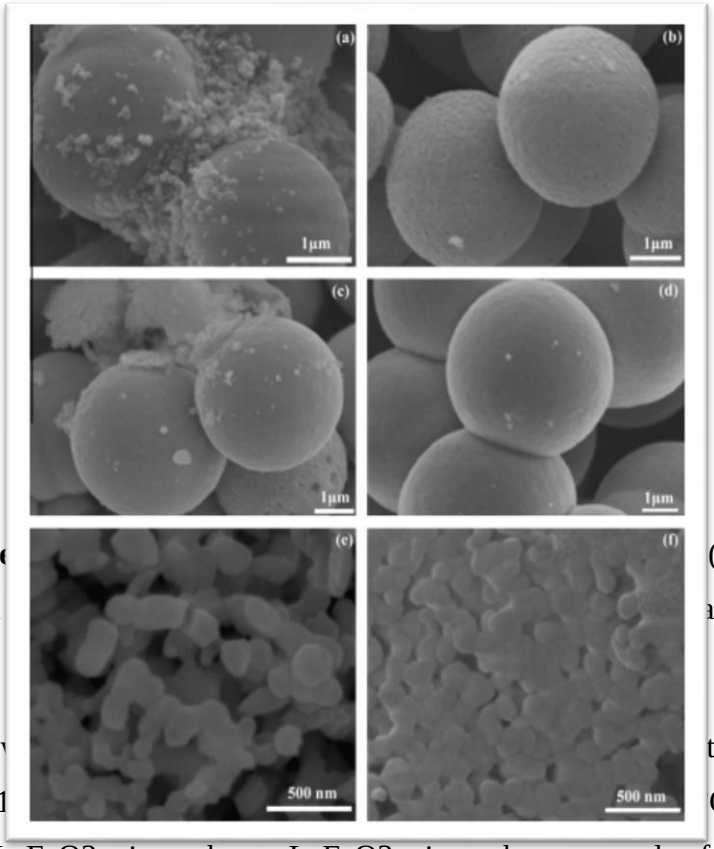

Figure (b) 12 h, (c) 18 h, (d) 24 h; high ally reacted at 180 °C.

Experiments t various periods, including 6, 1 C, to explore the formation of LaFeO3 microspheres. LaFeO3 microspheres started to form after 6 hours, despite the presence of a few aggregated nanoparticles, showing that the self-assembly of nanoparticles is what causes the creation of LaFeO3 microspheres (**Figure III.12a**). The SEM picture at 12 hours (**Figure III.12b**) reveals smooth-surfaced microspheres with diameters between 2 and 3 m and an average size of 70 nm. Based on these findings, the nucleation, development, and aggregation of nanoparticles is the most likely mechanism for microsphere growth. The size of the microspheres expanded, reaching a diameter of 3.5–4.5 m as the reaction time rose to 18 hours (**Figure III.12c**). A dissolution-recrystallization process, which is frequently seen in hydrothermal synthesis of nanomaterials, was also indicated by a few aggregated tiny particles that

were discovered on the surface of the microspheres. Individual microspheres were destroyed when the reaction time was extended to 24 hours (**Figure III.12d**), resulting in the development of composite microspheres. This shows that the 18-hour-old nanoparticles were devoured, showing that the Ostwald ripening mechanism and reassembly process were in use in this instance.

❖ Solid state method

works by Thiruvenkadam Vijayaraghavan, Ramanathan Sivasubramanian, Shamima Hussain, and Anuradha Ashok[5,6]

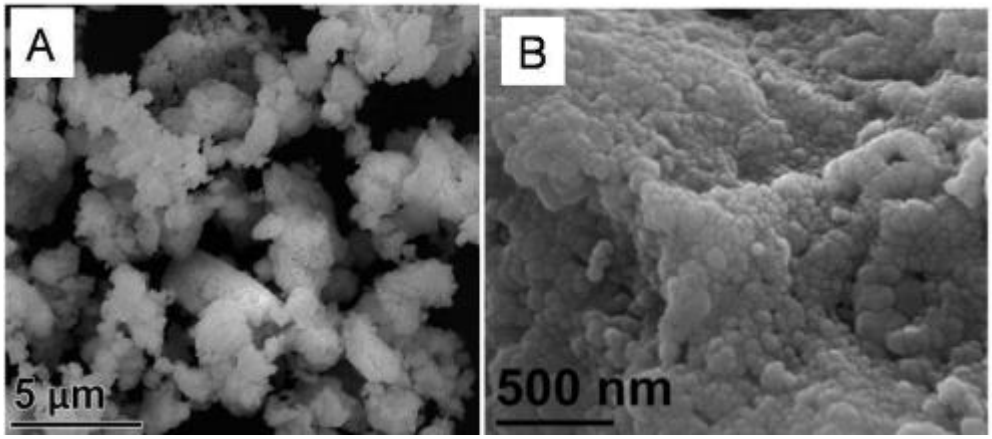

Figure.III.13: (A&B) SEM images at different magnifications

Through SEM examinations, the surface morphology of LaFeO3 powder was examined. The LaFeO3 SEM images of **Figure III.13** (A & B) were taken at various magnifications. The aggregated structure of the particles has an average size of about 45 nm. Higher magnification of **Figure III.13** (B) reveals a cauliflower-like shape, indicating the presence of several agglomerated nanocrystallites with distinct borders.

III. 4 :Use a compound in the following methods $LaFeO_3$.

The use of LaFeO3 in the Sol-Gel technique is advantageous in many different fields. It functions as an optical stimulation catalyst, improving light responsiveness and signal conversion into quantifiable electrical impulses. LaFeO3 is also used in the production of solid oxide fuel cells, solar cells, and other electronic and sensing devices.

Chapter III: Synthesis and characterization of LaFeO3 oxide and discussion of the biblio results graphically

The use of LaFeO3 in the hydrothermal process exhibits good photocatalytic activity. It works as a stimulating substance to quicken photocatalytic reactions, boosting the effectiveness of these chemical processes and making it easier to turn light components into useful products.

A variety of significant applications are demonstrated by the usage of the LaFeO3 molecule in the solid-state approach. It works well as a catalyst in batteries, improving battery performance and expanding their capacity for energy storage and release. Additionally, it helps to improve important electrochemical reactions by acting as a very effective electrical catalyst in applications like fuel cells. LaFeO3 is also used to detect and analyze chemical substances and gases in electrochemical sensing equipment.

Reference

[1] Theingi, Mya, Kay Thi Tun, and Nwe Nwe Aung. "Preparation, characterization and optical property of LaFeO3 nanoparticles via sol-gel combustion method." *SciMedicine Journal* 1.3 (2019): 151-157.

[2] Tapouk, Fahim Amini, et al. "Synthesis of PAC-LaFeO3-Cu nanocomposites via sol-gel method for the photo catalytic degradation of humic acids under visible light irradiation." *Journal of Environmental Chemical Engineering* 9.4 (2021): 105557.

[3] Thirumalairajan, S., et al. "Controlled synthesis of perovskite LaFeO3 icrosphere composed of nanoparticles via self-assembly process and their associated photocatalytic activity." *Chemical Engineering Journal* 209 (2012): 420-428.

[4] Wang, Boqun, et al. "Gas sensing with yolk-shell LaFeO3 microspheres prepared by facile hydrothermal synthesis." Sensors and Actuators B: Chemical 258 (2018): 1215-1222.

[5]Vijayaraghavan, Thiruvenkadam, et al. "A facile synthesis of LaFeO3-based perovskites and their application towards sensing of neurotransmitters." *ChemistrySelect* 2.20 (2017): 5570-5577.

[6] Sazelee, N. A., et al. "LaFeO3 synthesised by solid-state method for enhanced sorption properties of MgH2." Results in Physics 16 (2020): 102844.

Chapter III: Synthesis and characterization of LaFeO3 oxide and discussion of the biblio results graphically

Chapter III: Synthesis and characterization of LaFeO3 oxide and discussion of the biblio results graphically

.

Chapter III: Synthesis and characterization of LaFeO3 oxide and discussion of the biblio results graphically

Chapter III: Synthesis and characterization of LaFeO3 oxide and discussion of the biblio results graphically

Chapter III: Synthesis and characterization of LaFeO3 oxide and discussion of the biblio results graphically

Chapter III: Synthesis and characterization of LaFeO3 oxide and discussion of the biblio results graphically

Chapter III: Synthesis and characterization of LaFeO3 oxide and discussion of the biblio results graphically

Chapter III: Synthesis and characterization of LaFeO3 oxide and discussion of the biblio results graphically

Chapter III: Synthesis and characterization of LaFeO3 oxide and discussion of the biblio results graphically

General Conclusion

General Conclusion:

In our work, we used three different approaches sol-gel, hydrothermal, and solid-state to compare the properties of the combination LaFeO3. We used a variety of methods to analyze the results, including XRD, FTIR, ATD/ATG, and SEM. Following our analysis of the data, we discovered the following comparisons:

Three different methods for preparing LaFeO3 were compared using X-ray diffraction (XRD). All methods resulted in the transformation of the material into LaFeO3 crystals. Different temperatures were used for each method. The sol-gel method showed a transformation into a crystalline perovskite structure with different crystal sizes. The hydrothermal method transformed the amorphous phase into crystalline LaFeO3 at a specific annealing temperature, with an increased peak intensity indicating improved crystallinity and microsphere growth. The solid-state method showed a high-quality crystalline perovskite structure with smaller crystal size. Further studies are needed to determine other properties such as electrical and optical characteristics for a comprehensive understanding of the overall material performance.

The samples were analyzed using FTIR. The sol-gel method showed absorptions indicative of carbon residues, while the hydrothermal method exhibited absorptions related to water molecules, carboxyl groups, and carbon dioxide absorption. In the solid-state method, absorptions associated with carbonyl groups and FeO vibrations were observed. All three methods showed absorptions related to vibrational patterns of functional groups or impurities present in the samples. Stretching vibrations such as O-H, C-O, C=O, and FeO stretching were observed in all methods.

The thermal analysis results of the sol-gel, hydrothermal, and solid-state methods reveal similarities and differences. All methods lead to the formation of LaFeO3, indicating successful synthesis. However, the decomposition reactions, weight loss patterns, and thermal behavior differ among the methods. The solid-state method exhibits the desired phase. In general, the Sol-Gel method can be considered the easiest to implement and control the process, while the solid-state method can be considered the best if the crystalline quality and crystal size are the priority. However, other criteria related to the study or application should be taken into consideration, as well as the availability of equipment, resources, and required expertise for each method, before making the final decision.

Finally, Due to the unavailability of materials and limited resources, our study was limited to theoretical analysis rather than practical applications. We acknowledge that conducting practical experiments and exploring the applications of each method would have provided more valuable results. We apologize for any confusion caused by the limited scope of our study and the absence of practical investigations.

ABSTRACT

This work is a theoretical study on the effect of various methods of preparing perovskite on its physical and chemical properties, as well as uses of $LaFeO_3$ in battery charge, solar cell manufacturing, and thermal stimulation, with a particular focus on comparing results with previous articles on $LaFeO_3$. First, we compared results obtained from the sol-gel method and hydrothermal treatment using X-r diffraction (XRD) to assess crystalline structure at 800 °C. On the other hand, the solid state method showed high-grade crystalline structure at 900 °C. Results of weight thermal analysis (TGA) and differential thermal analysis (DTA) indicated active peaks at 800 °C in the sol-gel and hydrothermal method, indicating similar degradation processes. In the solid state method, an active peak is observed at 900 °C. Using FTIR technology, all three methods showed absorption associated with the vibrational patterns of functional groups, with the expansion of the O-H, C-O, and C = O bonds. Our study revealed that sol-gel method is the easiest, most used, and least expensive method, providing the most accurate results

Key words: perovskite, sol-gel method, $LaFeO_3$, X-ray diffracti

الملخص

هذا العمل عبارة عن دراسة نظرية حول تأثير الطرق المختلفة لإعداد البيروفسكايت على خصائصه الفيزيائية والكيميائية، بالإضافة إلى استخدامات $LaFeO_3$ في شحن البطاريات وتصنيع الخلايا الشمسية والتحفيز الحراري، مع التركيز بشكل خاص على مقارنة النتائج مع المقالات السابقة حول $LaFeO_3$. أولاً، قارنا النتائج التي تم الحصول عليها من طريقة sol-gel والمعالجة الحرارية المائية باستخدام حيود X-R (XRD) لتقييم البنية البلورية عند 800 درجة مئوية. من ناحية أخرى، أظهرت طريقة الحالة الصلبة بنية بلورية عالية الدرجة عند 900 درجة مئوية. أشارت نتائج التحليل الحراري للوزن (TGA) والتحليل الحراري التفاضلي (DTA) إلى قمم نشطة عند 800 درجة مئوية في طريقة هلام السول والحرارة المائية، مما يشير إلى عمليات تحلل مماثلة. في طريقة الحالة الصلبة، يتم ملاحظة ذروة نشطة عند 900 درجة مئوية. باستخدام تقنية FTIR، أظهرت الطرق الثلاث امتصاصًا مرتبطًا بالأنماط الاهتزازية للمجموعات الوظيفية، مع توسيع روابط O-H و C-O و C = O. كشفت دراستنا أن طريقة sol-gel هي الطريقة الأسهل والأكثر استخدامًا والأقل تكلفة، مما يوفر النتائج الأكثر دقة

الكلمات المفتاحية: البيروفسكايت , $LaFeO_3$, سول -جال ,التحليل الحراري, الاشعة السينية

RESUME

Ce travail est une étude théorique sur l'effet de diverses méthodes de préparation de perovskite sur ses propriétés physiques et chimiques, ainsi que les utilisations de $LaFeO_3$ en charge de batterie, fabrication de cellules solaires, et la stimulation thermique, avec un accent particulier sur la comparaison des résultats avec les articles précédents sur $LaFeO_3$. Tout d'abord, nous avons comparé les résultats obtenus par la méthode sol-gel et le traitement hydrothermique à l'aide de la diffraction X-r (XRD) pour évaluer la structure cristalline à 800 °C. D'autre part, la méthode à l'état solide a montré une structure cristalline de haute qualité à 900 °C. Résultats de l'analyse thermique du poids (TGA) et l'analyse thermique différentielle (DTA) ont indiqué des pics actifs à 800 °C dans la méthode sol-gel et hydrothermique, indiquant des processus de dégradation similaires. Dans la méthode à l'état solide, un pic actif est observé à 900 °C. En utilisant la technologie FTIR, les trois méthodes ont montré une absorption associée aux modèles vibratoires des groupes fonctionnels, avec l'expansion des liaisons O-H, C-O et C = O. Notre étude a révélé que la méthode sol-gel est la plus facile, la plus utilisée et la moins coûteuse, fournissant les résultats les plus précis.

Mots clés: perovskite, méthode sol-gel, $LaFeO_3$, diffraction des rayons X